https://doi.org/10.1016/j.matchemphys.2016.04.004

Laser fabrication of W-reinforced Cu layers: II. Electrical wear behavior in air and synthetic acid rain

P.K. Wong[a], C.T. Kwok[a,b], H.C. Man[c], D. Guo[a]

[a] Department of Electromechanical Engineering, University of Macau, China

[b] Institute of Applied Physics and Materials Engineering, University of Macau, China

[c] Department of Industrial and Systems Engineering, The Hong Kong Polytechnic University, Hong Kong, China

Abstract

In order to enhance the electrical sliding wear resistance and hence the lifespan of cp Cu for applications in electrical contacts, W-reinforced Cu layers were fabricated by laser surface modification on cp Cu. Compared with cp Cu, the hardness of the laser-fabricated layers with 55 to 60 wt% W was improved from 70 to 150 $HV_{0.2}$ while electrical wear resistances in dry and wet conditions were improved by 3 orders of magnitude despite the increase in the interfacial contact resistance of the layers. The main contribution of electrical wear in synthetic acid rain is mechanical wear, with contribution of corrosion-wear synergism up to 32.8%, while corrosion alone is negligible.

Key words: alloys; coatings; SEM; hardness; wear

1. Introduction

During running of railway trains, a copper current collector or contact strip slides along the overhead copper wires or steel third rails to transfer electrical power to the

trains. The efficiency of a power collection system depends on the conductive performance of the materials and the quality of electrical contacts, which are affected by many parameters, such as the speed of rain, electric current, load, contact dynamics and atmospheric conditions [1-3]. The electric current in a sliding couple influences their surface temperature, erosion and oxidation characteristics [4-6]. Electric current has a significant effect on the frictional coefficient and wear rate of the contact materials owing to Joule heating and arc discharges [7]. Moreover, the effect of environment conditions also plays a crucial role in affecting the service life of sliding couples. Railway electrification systems operate in a variety of weather conditions, such as dry, wet, acid rain, fog and even snow. Thus the electrical erosion properties of the contact parts are influenced by such conditions. Therefore, study on the electrical sliding wear of the contact materials under different environment conditions is necessary.

Laser surface modification involves the mixing of pre-/co-deposited material with the underlying substrate to form a tailor-made material which is difficult to obtain by other methods. It is a feasible technique for fabricating coatings and repairing undersized and worn electric contact components, especially at localized regions suffering from electrical sliding wear. It can be used to substitute expensive powder metallurgical process, for which it is not easy to control the degree of compaction and hence the electrical conductivity of the contact materials is deteriorated. In order to enhance the hardness, wear resistance and hence the service life of copper as electrical contacts, Ng and his co-workers reported that laser cladding of Ni (intermediate layer) and Mo (top layer) on Cu as a sandwich layer of Mo/Ni/Cu using 2.5-kW CW Nd:YAG laser was successfully fabricated for overcoming the difficulties arising from the large difference in thermal properties and the low mutual solubility between Cu and Mo [8]. The hardness of the surface of the

clad layer is 7 times higher than that of the Cu substrate. Pin-on-disc wear tests also showed that the abrasive wear resistance of the clad layer was also improved by a factor of 7 as compared with the Cu substrate. On the other hand, Li and his co-worker reported that the average hardness of the Cu laser-modified with NiCrFeSiBC by a 5-kW CW CO_2 laser was increased to 650 HV, and the wear rate in a block on ring test against hardened steel was reduced by 0.8 as compared with Cu [9]. This could be attributed to the presence of boride and carbide, grain refinement and solid solution strengthening in the modified layer. The electrical conductivity of the integral bulk was slightly affected by laser surface modification. While W-Cu composites combine the high hardness, high-temperature strength and excellent resistance to wear of W and the excellent electrical conductivity of Cu and is an attractive electrical contact material. Chu et al reported the high hardness and wear resistance of Cu–W films on Cu fabricated by RF magnetron sputter deposition was attributed to the fine structure and presence of W [10]. Compared with other insoluble elements such as Mo, Ta and C, W at 11.1 at% (26.5 wt%) in the films resulted in a highest wear resistance. However, the above studies mainly focused on dry wear while electrical sliding wear with corrosive media behavior was not investigated.

Electrical sliding wear of contact materials in corrosive media involves mechanical and electrochemical/chemical effects and their synergism. The total material removal rate can be more than the sum of the wear rates measured in the absence of corrosion and the corrosion rate observed in absence of wear [11]. Fathollahzade and Raeissi reported that the proportion of mass transport in tribocorrosion of electrodeposited Co-W coatings on Cu substrate conducted by a ball-on-plate tribometer in 3.5 wt-% NaCl solution at open-circuit potential and room temperature was higher than wear accelerated corrosion, which implied that the corrosion reaction of the coatings was mainly a mass transport controlled process [12].

Electrical wear behavior of copper [13-15], its alloys [16-18] and its composites [5, 21-24] in dry condition have been extensively studied. Acid rain is a natural electrolyte which often causes adverse corrosive effects on the electric contact materials used in outdoor environments. However, the electrical wear behavior of laser-fabricated W-reinforced Cu layers in the presence or absence of acidic rain water has not been reported in literature. In Part I of this article, the microstructure and corrosion behavior of laser-fabricated W-reinforced Cu layers in simulated acid rain (SAR) in static condition have been reported [25]. Compared with cp Cu, the corrosion current density of the laser-fabricated W-reinforced Cu layers in SAR at 25 ^{o}C was lower despite the active shift in open-circuit potential. From the corrosion morphology after immersion test in SAR, the Cu binder phase of the laser-fabricated specimens was selectively attacked, leading to dislodgement of the W particles. In Part II, the electrical sliding wear behavior of the laser-fabricated W-reinforced Cu layers in dry (in air) and wet conditions, i.e. in distilled water (DW) and SAR was evaluated.

2. Experimental details

2.1 Specimens preparation

Details on preparation of the laser-fabricated specimens of W-reinforced Cu layers have been described in Part I. The laser-fabricated specimens and cp Cu for electrical sliding wear testing were in the form of rectangular plates with dimensions of 22 mm x 19 mm x 6.3 mm. Surface of the specimens were ground with 400-grit SiC paper to remove surface oxide and then ultrasonically cleaned in ethanol followed by washing in distilled water for electrical sliding wear testing. cp Cu was used for comparison purpose.

2.2 Hardness and interfacial contact resistance (ICR) measurements

The overall hardness of laser-fabricated layers and local hardness at the specific phases (W or Cu) were measured using a microhardness tester with loads of 200 g and 25 g, respectively, and a loading time of 10 s. For each specimen, five different locations were selected for the hardness measurement and average hardness values were then calculated. The experimental error of microhardness data was of the order of 5%. Fig. 1 shows the schematic diagram of the interfacial contact resistance (*ICR*) measurement which has been previously described [26]. The laser-fabricated specimen was machined to a square plate with surface area of 10 mm × 10 mm. Compression force of 15 to 110 N/cm^2 was applied by a motorized force tester (LTCM-500, Chatillon) and the resistance was measured by connecting two Cu plates with a DC ohmmeter with an accuracy of ±1 μΩ (GOM-802, Gwinstek). The schematic diagram for measuring the *ICR* for laser-fabricated specimen is shown in Fig. 1. The total measured resistance is the sum of two interfacial components. For cp Cu without the laser-fabricated layer, the two interfacial components are the same, that is two cp Cu/Cu plate interfaces ($2R_{Cu/Cu}$); whereas for the laser-fabricated specimen, the interfacial components consists of a cp Cu (substrate)/Cu plate interface ($R_{Cu/Cu}$) and a laser-fabricated layer/Cu plate interface (R_c). The calculation of *ICR* of the laser-fabricated layer/Cu plate interface is shown in equation (1).

$$R_c = R_m - R_{Cu/Cu} \qquad (1)$$

where R_c = *ICR* of the laser-fabricated layer/Cu plate interface; R_m = measured resistance by the ohmmeter; $R_{Cu/Cu}$ = *ICR* of Cu/Cu plate interface, which is a constant at a fixed compression force.

2.3 Electrical sliding wear testing

Electrical sliding wear testing was conducted using a pin-on-disc tribometer as

shown in Fig. 2. The disc with diameter of 420 mm and thickness of 12 mm was attached to a spindle driven by a 7.5-kW variable-frequency high-speed electrical motor. The electric current applied on the specimens (the pins) was provided by a DC power supply as the cathode. A normal load of 50 N was applied to the specimens for maintaining the contact with the disc by a hydraulic press. The specimens were forced to slide against a counterface tool steel rotating disc with hardness of 600 $HV_{0.2}$. In a third rail system, Cu is used as the current collector shoes and steel is used as the third rail for providing electric power. Moreover, the iron-base contact strips (pantograph) were used in some catenary systems [16]. In this study, tool steel was selected because it is much harder than the laser-fabricated specimens and wear mainly occurs at the specimens. The sliding speeds of the disc were 40 and 60 km/h, without current and with DC current (60 A) under dry condition (in air) and wet conditions: with DW (pH 7) and SAR (pH 3.5).

The total sliding distances for cp Cu and the laser-fabricated specimens were 1 km and 6 km respectively. In dry condition, the tests were conducted at ambient temperature (25 ^{o}C) and a relative humidity of 60%. For simulating the acid rain, SAR was prepared with compositions of SO_4^{2-} 15.2 mg/L, NO_3^{-} 11 mg/L, Cl^{-} 27.3 mg/L, Na^{+} 27.3 mg/L, Ca^{2+} 5.5 mg/L, H^{+} = 0.3 mg/L at pH 3.5 [27]. DW or SAR was dropped to the proximity of the contact surface at a constant flow rate of 0.5 mL/s. Due to the presence of electric current and water, electric arc was produced leading to arc erosion (Fig. 2c). During the electrical wear test, the weight loss ΔW (in g) of the specimens was intermittently recorded at a time interval of 1 minute (for sliding at 60 km/h) or 1.5 minute (for sliding at 40 km/h) using an electronic balance with an accuracy of $\pm$0.1 mg. All the electrical wear tests were repeated three times to ensure the repeatability of the experimental data at the same testing conditions.The experimental error of weight loss data was of the order of 10.5%. The average wear

loss (thickness loss) Δd was then calculated by:

$$\Delta \mathrm{d\,(mm)} = 10\frac{\Delta \mathrm{W}}{\rho A} \qquad (1)$$

where ρ (in g/cm^3) and A (in cm^2) are the density and the exposed surface area of cp Cu or the laser-fabricated layers respectively. The densities of the laser-fabricated layers (Table 1) were calculated according to the weight fractions of Cu and W by the rule of mixture:

$$\rho(g/cm^3) = \rho_{Cu} W_{Cu} + \rho_{\mathrm{W}} \mathrm{W_W} \qquad (2)$$

where ρ_{Cu} = 8.9 g/cm^3 and ρ_W = 19.3 g/cm^3 are the theoretical densities of Cu and W respectively, and the corresponding weight fractions of Cu and W in the laser-fabricated W-Cu layer are W_{Cu} and W_W respectively ($W_{Cu} = 1 - W_W$).

The average rates of wear loss of materials are expressed in terms of the wear rate in dry condition (D), wear rate in DW without electrochemical corrosion (E) and wear-corrosion rate in SAR (T) respectively and calculated by the following equations:

$$\mathrm{Wear\ rate\ (mm/h)} = \frac{\Delta d}{\Delta t} \qquad (3)$$

where Δt (in h) is the duration of the wear test.

Synergistic effect between electrical wear and corrosion of the laser-fabricated specimens in SAR was analyzed. To investigate the synergism between electrical wear corrosion, wear-corrosion synergism S is calculated according to the following equation [28, 29]:

$$S = T - E - C \qquad (4)$$

where C is the corrosion rate of the specimens in SAR calculated from the I_{corr} obtained in Part I according to ASTM Standard G102-89 [30]:

$$\mathrm{C\,(mm\ yr^{-1})} = K\left(\frac{I_{corr}}{\rho}\right)\mathrm{EW} \qquad (5)$$

where K is a constant = 3.27 x 10^{-3} mm g μA^{-1} cm^{-1} yr^{-1}; I_{corr} is the corrosion current

density in μA cm^{-2}; ρ is the density obtained from equation (2) in g cm^{-3} (see Table 1); and EW is the equivalent weight, which is defined as follows:

$$\mathrm{EW} = \left(\Sigma \frac{n_i W_i}{A_i} \right)^{-1} \qquad (6)$$

where W_i is the weight fraction; n_i is the valence; and A_i is the atomic mass of the i^{th} element in the specimen.

After electrical sliding wear tests, the worn surface and debris from the specimens were analysed by scanning-electron microscopy (SEM, Hitachi S-3400N) and energy dispersive X-ray spectrometry (EDX, Horiba EX-250), while phase constitution was identified using X-ray diffractometry (XRD, Rigaku MiniFlex 600) with CuKα radiation operating at 40 kV and 15 mA at a scan rate was 0.1 ^{o}/s.

3. Results and Discussion

3.1 Hardness

The average hardness of Cu and W phases in the laser-fabricated specimens are 75 $HV_{0.025}$ and 378 $HV_{0.025}$ respectively (Table 1). The average hardness of W particles is 5.4 times that of the Cu binder. The overall surface hardness of the laser-fabricated specimens increases from 75 $HV_{0.2}$ to 150 $HV_{0.2}$. The laser-fabricated layers show increased hardness due to dispersion strengthening by hard W particles and micro-stresses induced [31] around the hard phase W (mismatch of thermal expansion coefficients between Cu [17 x 10^{-6} (^{o}C)$^{-1}$] and W [4.5 x 10^{-6} (^{o}C)$^{-1}$].

3.2 Electrical sliding wear behavior

The plots of cumulative wear (thickness) loss against distance traveled for the laser-fabricated specimens and cp Cu at different sliding speeds (40 and 60 km/h) under dry and wet (DW and SAR) conditions are shown in Fig. 3. The values of

average wear rates in different test conditions (*D*, *E* and *T*), wear-corrosion synergism (S) and corrosion rate in SAR (*C*) are summarized in Fig. 4 and Table 2. It can be observed that the wear rates increase with increasing sliding speed and current intensity due to arc discharge [15]. Indeed, all wear rates of the laser-fabricated specimens are much lower than that of cp Cu by about 3 orders of magnitude indicating that the W phase is very effective in resisting removal of surface materials. The plot of wear rate vs hardness for the laser-fabricated specimens and cp Cu at 60 km/h and 60 A in dry and wet conditions is shown in Fig. 5. The laser-fabricated specimens show significant reduction in wear rates (*D*, *E* and *T*) in different test conditions due to higher hardness. Moreover, the presence of tungsten oxide film on the surface of the specimen as a result of oxidation during the electrical wear process could effectively reduce abrasion and adhesion with the steel disc and hence reduce the wear loss [32]. The ranking of electrical sliding wear resistance in dry and wet (DW and SAR) conditions is:

$$\text{LA-W-Cu-p2} \sim \text{LA-W-Cu-p1.8} \gg \text{cp Cu}$$

Generally, the ranking of wear rates in different conditions, corrosion rate in SAR and synergism are as follows:

$$D > T > E > S \gg C$$

C is much smaller than the wear rates (*D, T* and *E*) while *S* shows some contribution to *T*.

3.2.1 In dry condition

In dry condition without electric current, material loss is attributed solely to mechanical wear (abrasive and adhesive) and oxidation. The laser-fabricated specimens and cp Cu are plastically deformed. During dry sliding at high speeds, the shearing and ploughing in the sliding contact is so rapid that the frictional heat is

generated much faster than it can be conducted away. In addition to oxidation, the temperature rise leads to a reduction in hardness and higher wear rate, conforming to the Archard's equation [33]:

$$\text{Wear rate} = \frac{kFv}{H} \qquad (7)$$

where k is the wear coefficient, F is the normal force, v is the sliding speed and H is the hardness of the material.

For cp Cu sliding against the counterface steel disc at 60 km/h and 60 A in dry condition, the wear damage is the most severe. Due to the worn debris, continuous parallel ploughing grooves in the direction of motion and a considerable extent of micro-cutting on the worn surface are observed [Fig. 6a(i)]. In addition, the presence of erosion pit confirmed the occurrence of arc erosion [Fig. 6a(i)]. Plastically deformed and elongated grains on the surface, cracking, and equiaxed grains in the inner region can be observed in the cross-section of the worn cp Cu [Fig. 6a(ii)]. The cracks at the deformed surface of cp Cu was caused either by work hardening or thermal cycling, and followed by material detachment and formation of abrasive debris. The hard abrasive debris (Cu_2O) (Fig. 7) and work-hardened Cu phase promoted severe abrasion. The debris had a flake-like morphology and severely deformed the surface of cp Cu, which was the dominant mechanical wear mechanism. The hard asperities adhering on the steel counterpart (Fig. 8) penetrated and cut deeply into the surface of cp Cu, resulting in a large amount of material removal.

In addition, the coefficient of friction (μ) in the presence of electric current (I) was reported to be higher than that without electric current [34, 35]. A solid surface has certain degree of roughness, so the actual contact area between the sliding couples for electrical conduction is the sum of the small areas which is only a very small fraction of the apparent contact area. Based on the theory of electric contact, current flow between sliding couples was restrained to the very small contacts area called 'a

spots' [36]. Consequently, the current density flowing through the individual 'a spots' may exceed the nominal value by many times. Thus for sliding surfaces with electric current both frictional heating and Joule heating are present. The total power loss P is the sum of electrical and mechanical loss [37]:

$$P = I^2 R_c + \mu v F \qquad (8)$$

where I is the electric current, R_c is the contact resistance, μ is the friction coefficient, v is the sliding speed and F is the normal load applied to the specimens. The combined effects of frictional heating and Joule heating from the applied current speeded up the specimens to reach its softening temperature, leading to decrease in hardness. The surface of cp Cu was softened (above 190 ^{o}C) and massive material transfer occurred, with adhesive Cu patches found on the counterface steel disc (Fig. 8). The worn debris then acted as free abrasive particles and ploughed the surface of cp Cu, demonstrating abrasive wear mechanism. The sliding surfaces were damaged and surface roughness was increased.

In addition to Joule heating, it is clearly observed that the wear rate is higher as the electric current increases owing to arc discharge (Fig. 4). With the increase in sliding speed and electric current, the contact surface temperature between the specimen and the disc increases quickly. The arc discharge also becomes stronger and results in the aggravated arc erosion on the surface of the specimens. The worn surface of the laser-fabricated specimens at 60 km/h and 60 A in dry conditions are shown in Fig. 9. Compared with cp Cu, a much lower degree of damage is observed on the surface of the laser-fabricated specimens. Plastic deformation can be observed in both Cu and W phases in the laser-fabricated specimens while the characteristic grooves are only observed in the Cu phase. The electrical wear resistance of the laser-fabricated specimens was enhanced by 3 orders of magnitude because the W phase possesses higher hardness and softening temperature (1000 ^{o}C) than the Cu

phase. LA-W-Cu-p2 is more wear resistant than LA-W-Cu-p1.8 owing to the higher W content in the former. Likewise, Tu and his co-workers reported that the wear resistance of the Cu-TiB_2 nanocomposites increased considerably with the content of TiB_2 nanoparticles [38]. Compared with the Cu phase (75 $HV_{0.025}$), the hardness of the W phase (378 $HV_{0.025}$) in the laser-fabricated specimens is higher. The overall hardness of LA-W-Cu-p2 (150 $HV_{0.2}$) is slightly higher than that of LA-W-Cu-p1.8 (138 $HV_{0.2}$) due to the higher W content in the former. The electrical wear resistance increases with the W content. The harder W phase can take up the applied load and reduce the amount of wear loss.

Hirose and Kobayashi reported that the Cu-Cr alloyed layer had 3 to 4 times the hardness of pure Cu at 600 ^{o}C [39]. It is believed that dispersion of the W phase in the Cu binder also strengthened the structure effectively at elevated temperatures since the softening temperature of Cu (190 ^{o}C) is much lower than that of W (1000 ^{o}C) [40]. Due to the higher hardness and higher softening temperature of W, plastic deformation of the laser-fabricated W-reinforced Cu layers was significantly reduced. During electrical wear, the effects of dislocation strengthening and grain refinement (due to deformation), solid solution strengthening (by alloying with Fe), particle strengthening (oxide particles), and composite strengthening (pick up of counter material or worn particles) could help strengthen the laser-fabricated W-reinforced Cu layers [41,42]. From Fig. 9, it can be seen that grooves and patches on the worn surfaces of the laser-fabricated specimens were mainly caused by abrasive and adhesive wear. Hard W and oxides phases were detached from the worn surfaces. The W phases were severely deformed and elongated and even broken into smaller pieces as shown in Fig. 9.

The presence of electric current increased surface temperature by Joule heating and enhanced oxidation. The metal oxide films fractured during abrasion, and

generated debris which further aggravated the wear damage. Ding and his co-workers reported that when normal stress was larger than or equal to the threshold value (0.64 MPa), friction coefficients increased with electric current, wear losses of the copper-impregnated metallized carbon material increased slightly with the increase of normal force, and contact resistance heat enhanced mechanical wear [24]. On the other hand, if the normal stress was smaller than the threshold value, friction coefficients decreased with increasing electric current, wear losses increased intensely due to arc heat and erosion. Sliding wear with adhesion and abrasion was the major damage mechanism of the frictional couples, but the material loss caused by arc erosion was much larger than those caused by adhesion and abrasion [24]. In the present study, the arc erosion was the dominant damage mechanism for the laser-fabricated specimens with a normal load of 0.15 MPa.

Due to Joule heating, sliding with electric current favored oxidation of both the specimen and the counterface steel disc. Bouchoucha *et al* reported that the transfer and oxidation phenomena occurred during electrical sliding of the surfaces of cp Cu and CrNi-steel in oxidizing medium [43]. Without current, the transfer of Cu phase was followed by oxidation. The predominant oxide was Cu_2O and the wear was of the oxidation type. With current up to 40 A, the degree of oxidation increased and the transferred elements were oxidized to form hard oxides (Cr_2O_3 and Fe_2O_3). Besides oxidation wear, abrasive wear was manifested. In the present study, metal oxides (Cu_2O, Fe_2O_3 and WO_2) were detected in the XRD patterns of the laser-fabricated specimens after wear tests (Fig. 10). This confirms that oxidation was contributive to subsequent damage of the contact surface. These oxides acted as hard abrasives in between the sliding contacts. Moreover, electrical sliding of the specimens against the steel disc could also induce the transfer of Fe to Cu or vice versa, as reflected by the small amount of Fe detected on the worn surface by EDS analysis [Fig. 9b(iii)].

BSE micrographs of the cross-sectional views of LA-W-Cu-p2 after electrical wear are shown in Fig. 9b(ii). After electrical wear test in dry condition, the thickness of laser-fabricated specimen (LA-W-Cu-p2) was reduced from 0.43 mm to 0.14 mm (for dry condition). A laminate structure (about 50-μm thick) with cracks can be observed on the top of the W-reinforced layers as shown in Fig. 9b(iii). The damage mechanism in dry condition was therefore associated with delamination fatigue. The schematic of wear mechanism of the laser-fabricated W-reinforced Cu layers is shown in Fig. 11. In the beginning, both Cu and W phases were severely deformed by the counterpart. Due to severe deformation, high-strain and thermal effects, the subsurface was mechanically alloyed with fine elongated W phases dispersed in the Cu-Fe-W matrix as a hardened laminate layer. In the laminate layer, finely crushed and elongated W phases (ranging from 0.5 to 10 μm) were dispersed in the matrix with compositions of Cu 55 wt%, W 32 wt%, Fe 4.9 wt%, O 8.4 wt%. The refined and elongated W phases in the laminate layer were nearly parallel to the worn surface. From Table 2, the worn surface (355 to 375 $HV_{0.2}$) of the laser-fabricated specimens in dry condition was harder than the non-worn surface (138 to 150 $HV_{0.2}$) due to severe deformation and mechanical alloying. Although this hardened laminate layer was resistant to electrical wear, it was less ductile than Cu and susceptible to micro-cracking. When the cracks joined together, fracture, delamination and material loss would occur from the surface of the laminate layers.

3.2.2 In wet conditions

As mentioned before, the wear rates in wet conditions (DW and SAR) are much smaller than that in dry condition (i.e. $D > T > E$) although the presence of electric current and water will enhance the production of electric arc. Morphologies of worn surfaces of cp Cu and the laser-fabricated specimens in with DW and SAR are shown

in Figs. 5b and c, 12 and 13. Under the wet conditions (in DW and SAR), the amount of adherent material on the surface of the steel disc decreased significantly compared with that in dry condition. Firstly, DW and SAR acted as lubricant with a boundary lubrication effect for reducing friction. Secondly, they also functioned as coolant to reduce the thermal effect, which otherwise might enhance the softening and plastic deformation of the materials.

Micro-plough and plastic deformation can be also observed on the surface of cp Cu eroded in DW and SAR but the degree of damage is less serious as compared with cp Cu eroded in dry condition (Fig. 5a). From the XRD pattern as shown in Fig. 6c, Cu_2O was also detected on the worn surface of cp Cu in SAR due to oxidation. Generally, the damage morphology for the laser-fabricated specimens is similar after wear test with DW (Fig. 12) and SAR (Fig. 13). The laminate layers of LA-W-Cu-p2 worn with SAR (about 16 μm) [Fig. 13b(ii)] were thinner than that of LA-W-Cu-p2 worn in dry condition [Fig. 8b(ii)]. There was a micro-crack formed in the laminate layer of LA-W-Cu-p2 eroded in SAR as depicted in Fig. 13b(iii). In SAR, the dominant wear mechanism for cp Cu and the laser-fabricated specimens was still adhesive and abrasive wear and delamination fatigue as evidenced by the presence of adherent material on the surface of the counterface disc, and by the presence of typical micro-plough and micro-cracks on the worn surface. For the laser-fabricated specimens worn in SAR, delineation at the boundaries between the W phase and the Cu binder can be observed, while the W phases were deformed and elongated as shown in Figs. 12-13. Compared with the laser-fabricated specimens before electrical wear test, higher-intensity α-Cu peaks were detected in the XRD patterns of the laser-fabricated specimens after electrical wear in dry (Fig. 10) and wet conditions (Fig. 14), reflecting that the loss of W phase was more than the Cu phase.

Assuming the lubricating effect of DW and SAR to be the same, the contribution

of E (in DW), C and S to total erosion rate T (in SAR) of the various specimens are summarized in Table 2. It can be seen that the contributions of E/T for all specimens are significant, indicating that wear loss is induced dominantly by mechanical and arcing effects. With the increase in corrosivity of the medium, the wear rate was higher ($T > E$). SAR can enhance the material loss by wear-corrosion synergism (S). The wear loss of the laser-fabricated specimens consisted of the delamination of brittle layer, detachment of worn debris and corrosion products. From the XRD patterns shown in Fig. 14a and b, Cu_2O was detected on the surface of the laser-fabricated specimens worn with DW but not detected in the ones worn in SAR. The corrosion products would be removed by wear and then the fresh surface would be further exposed to the SAR. According to Part I of this article, the passivity of W in the laser-fabricated specimens eroded with SAR enhanced the preferential dissolution of Cu binder, which started at the phase boundaries and propagated into the Cu phase according to the following anodic reaction ($Cu \rightarrow Cu^{2+} + 2e^-$). In the SAR with the presence of air, dissolved O_2 promoted dissolution of Cu by providing the following cathodic reaction ($O_2 + 4H^+ + 4e^- \rightarrow 2H_2O$). With SAR, the electrical wear rate of the laser-fabricated specimens was accelerated due to the synergistic effect of mechanical wear, arc erosion, and corrosion caused by SAR.

3.3 Worn debris

Worn debris with elongated W phase in Cu binder from the laser-fabricated specimens after electrical wear test in dry condition and SAR are depicted in Fig. 15. It can be noted that the debris have large size (about 500 μm). EDX analyses for the pulled-out debris show that they mainly consist of Cu, W, Fe and O. It is similar to the compositions of the laminate layers (Cu-Fe-W) and plays an important part in keeping

its high hardness under dry and wet conditions [Fig. 9b(iii)].

3.4 Interfacial contact resistance

The plot of *ICR* of cp Cu and the laser-fabricated specimens versus applied compressive force is shown in Fig. 16 and the steady values of *ICR* at 50 N/cm^2 are listed in Table 1. The ranking of *ICR* values is:

LA-W-Cu-p2 > LA-W-Cu-p1.8 > cp Cu

Compared with cp Cu, the *ICR* of LA-W-Cu-p1.8 and LA-W-Cu-p2 at 50 N/cm^2 increased by factors of 6 and 17 respectively. It seems that the *ICR* increased with the increase in W content, which was due to the higher electrical resistance of the W phase present in the laser-fabricated layers. Although the *ICR* of LA-W-Cu-p2 was higher than that of LA-W-Cu-p1.8, the former had higher electrical wear and corrosion resistances in all the testing conditions.

4. Conclusions

- The average hardness of Cu and W phases in the laser-fabricated specimens are 70 and 378 $HV_{0.2}$ respectively. The laser-fabricated layers show increased hardness mainly due to dispersion strengthening of harder W particles in the Cu matrix.
- Due to higher hardness and higher softening temperature of the W phase, the electrical wear resistance of the laser-fabricated layers is increased by 3 orders of magnitude as compared with cp Cu.
- The ranking of electrical wear resistance in dry and wet (distilled water and synthetic acid rain) conditions is:

  LA-W-Cu-p2 ~ LA-W-Cu-p1.8 >> cp Cu
- The wear rates in dry and wet conditions increase with sliding speed and electrical current. Generally, the wear rates of the specimens in different

conditions are as follows:

$$D > T > E > S >> C$$

- The main contribution of electrical wear in SAR is mechanical wear, with contribution of wear-corrosion synergism up to 32.8%, while corrosion alone is negligible.
- Interfacial contact resistance of the laser-fabricated layers increases with the increase in W content due to the higher electrical resistance of the W.

Acknowledgements

The work described in this manuscript was fully supported by research grants from the Science and Technology Development Fund (FDCT) of Macau SAR (Grant no. FDCT 070/2011/A3).

References

[1] C.R.F. Azevedo, A. Sinatora, Engineering Failure Analysis 11 (2004) 829.

[2] A. Senouci, H. Zaidi, J. Frene, A. Bouchoucha, D. Paulmier, Appl. Surf. Sci. 144-145 (1999) 287.

[3] D.H. He, H. R. Manory, Wear 249 (2001) 626.

[4] H. Zaidi, K. J. Chin, J. Frene, Surface and Coatings Technology, 148 (2001) 241.

[5] S. Kubo, K. Kato, Tribology International, 32 (1999) 367.

[6] Z. Chen, P. Liu, J.D. Verhoeven, E.D. Gibson, Wear, 203-204 (1997) 28.

[7] S. Kubo, K. Kato, Wear, 216 (1998) 172.

[8] K.W. Ng, H.C. Man, F.T. Cheng, T.M. Yue, Appl. Surf. Sci. 253 (2007) 6236.

[9] M. Li, M. Chao, E. Liang, J. Yu, J. Zhang, D. Li, Appl. Surf. Sci. 258 (2011) 1599.

[10] J.P. Chu, C.J. Liu, C.H. Lin, T.N. Lin, S.F. Wang, Mater. Chem. Phys. 72 (2001)

286

[11] P. Jemmely, S. Mischler, D. Landolt, Wear 237 (2000) 63.

[12] N. Fathollahzade, K. Raeissi, Materials Chemistry and Physics 148 (2014) 67.

[13] T. Ding, G.X. Chen, J. Bu, W.H. Zhang, Wear 271 (2011) 1629.

[14] A. Bouchoucha, S. Chekroud, D. Paulmier, Mater. Chem. Phys. 223 (2004) 330.

[15] H.J. Yang, G.X. Chen, G.Q. Gao, G.N. Wu, W.H. Zhang, Wear 332–333 (2015) 949.

[16] H. Nagasawa, K. Kato, Wear, 216 (1998) 179.

[17] S.G. Jia, P. Liu, F.Z. Ren, B.H. Tian, M.S. Zheng, G.S. Zhou, Wear 262 (2007) 772.

[18] Y.A. Wang, J.X. Li, Y. Yan, L.J. Qiao, Tribology International 50 (2012) 26.

[19]J.P. Tu, W.X. Qi, Y.Z Yang, F. Liu, J.T. Zhang, G.Y. Gan, N.Y. Wang, X.B. Zhang, M.S. Liu, Wear 249 (2001) 1021.

[20] S.G. Jia, P. Liu, F.Z. Ren, B.H. Tian, M.S. Zheng, G.S. Zhou, Mater. Sci. Eng. A398 (2005) 262.

[21] R.G. Zheng, Z.J. Zhan, W.K. Wang, Wear 268 (2010) 72.

[22] J. Yin, H. Zhang, C. Tan, X. Xiong, Wear 312 (2014) 91.

[23] X.C. Ma, G.Q. He, D.H. He, C.S. Chen, Z.F. Hu, Wear, 265 (2008) 1087.

[24] T. Ding, G.X. Chen, M.H. Zhu, W.H. Zhang, Z.R. Zhou, Wear 267 (2009) 1080.

[25] P.K. Wong, C.T. Kwok, H.C. Man, D. Guo, Laser fabrication of W reinforced Cu layers: I. Corrosion behavior in 3.5% NaCl solution and synthetic acid rain, submitted to Materials Chemistry and Physics.

[26] H.L. Wang, M.A. Sweikart, J.A. Turner, Journal of Power Sources 115 (2003) 243.

[27] Annual air quality report, Macao Meteorological and Geophysical Bureau, Macao Special Administration Region, 2010.

[28] Standard Guide for Determining Synergism Between Wear and Corrosion, G119-04, Annual Book of ASTM Standards, vol. 03.02, ASTM, Philadelphia, 2004.

[29] C.T. Kwok, F.T. Cheng, H.C. Man, Surface and Coatings Technology 145 (2001) 206.

[30] Standard Practice for Calculation of Corrosion rates and Related Information from Electrochemical Measurement, G102-89, Annual Book of ASTM Standards, Vol. 03.02, ASTM, Philadelphia, 1995.

[31] B.S. Yilbas, C. Karatas, Halil Karakoc, B.J. Abdul Aleem, S. Khan, N. Al-Aqeeli, Optics & Laser Technology, 66 (2015) 129.

[32] T. Polcar, N.M.G. Parreira, A. Cavaleiro, Vacuum 81 (2007) 1426–1429

[33] N.P. Suh, Tribophysics, Prentice-Hall, Englewood Cliffs, NJ, 1986.

[34] A. Shinchi, Y. Imada, F. Honda, K. Nakajima, Wear 230 (1999) 78.

[35] M.D. Bryant, IEEE Trans. Components Hybrids Manuf. Technol. 14 (1991) 71.

[36] P.G. Slade, Electrical Contacts: Principles and Applications, CRC, New York, 1999.

[37] P. Haney, D. Kuhlmann-Wilsdorf, H. Wilsdorf, Wear 73 (1981) 261.

[38] J.P. Tu, W. Rong, S.Y. Guo, Y.Z. Yang, Wear 255 (2003) 832

[39] A. Hirose, K.F. Kobayashi, Mater. Sci. Eng. A174 (1994) 199.

[40] M. Braunovic and N.K. Myshkin, Electrical Contacts: Fundamentals, Applications and Technology, CRC Press, NY (2007) p.72.

[41] S. Asadi Kouhanjani, A. ZareBidaki, A. Akbari, J. Alloy. Compd. 486 (2009) 319.

[42] S. Jacobson, S. Hogmark, Wear 266 (2009) 370.

[43] A. Bouchoucha, E.K. Kadiri, F. Robert, H. Zaidi, D. Paulmier, Surf. Coat. Tech. 76-77 (1995) 521.

Table

Specimen	W content (W_w) (wt%)	Density (g/cm^3)	Average hardness			Average hardness after wear test under dry condition 60 km/ 60A ($HV_{0.2}$)	Average hardness after wear test with SAR 60 km/ 60A ($HV_{0.2}$)	ICR (mΩ·cm^2) at 50 N/cm^2
			Cu phase ($HV_{0.025}$)	W phase ($HV_{0.025}$)	Overall ($HV_{0.2}$)			
cp Cu	0	8.9	-	-	75	95	97	0.031
LA-W-Cu-p1.8	55	14.6	75	378	138	355	398	0.363
LA-W-Cu-p2	60	15.2	75	378	150	375	404	1.117

Table 1. W content, density, hardness and interfacial contact resistance (ICR) of cp Cu and laser-fabricated specimens before and after electrical sliding wear test.

Specimen	Test conditions	Wear rate (mm/h)					Contribution (%)		
		D	*E* (in DW)	*T* (in SAR)	C (in SAR) (10^{-6})	S	E/T	S/T	C/T (10^{-6})
LA-W-Cu-p1.8	40km/h 0A	0.43	0.22	0.33	1.92	0.11	66.67	33.33	581.82
LA-W-Cu-p2		0.51	0.18	0.25	1.18	0.07	72.00	28.00	472.00
cp Cu		165.45	129.49	151.11	4.16	21.62	85.69	14.31	2.75
LA-W-Cu-p1.8	40km/h 60A	0.58	0.33	0.35	1.92	0.02	94.29	5.71	548.57
LA-W-Cu-p2		0.45	0.25	0.35	1.18	0.10	71.43	28.57	337.14
cp Cu		192.19	177.18	185.93	4.16	8.75	95.29	4.71	2.24
LA-W-Cu-p1.8	60km/h 0A	1.14	0.41	0.50	1.92	0.09	82.00	18.00	384.00
LA-W-Cu-p2		0.87	0.41	0.46	1.18	0.05	89.13	10.87	256.52
cp Cu		278.91	213.62	220.94	4.16	7.32	96.69	3.31	1.88
LA-W-Cu-p1.8	60km/h 60A	1.15	0.55	0.62	1.92	0.07	88.71	11.29	309.68
LA-W-Cu-p2		1.01	0.44	0.56	1.18	0.12	78.57	21.43	210.71
cp Cu		292.92	222.85	259.67	4.16	36.82	85.82	14.18	1.60

Table 2. Wear rates and relative contributions of *E, S* and *C* of laser-fabricated specimens and cp Cu.

Tables

Table 1. W content, density and hardness of cp Cu and laser-fabricated specimens before and after electrical sliding wear test.

Table 2. Wear rates and relative contributions of *E, S* and *C* of laser-fabricated specimens and cp Cu.

Figure

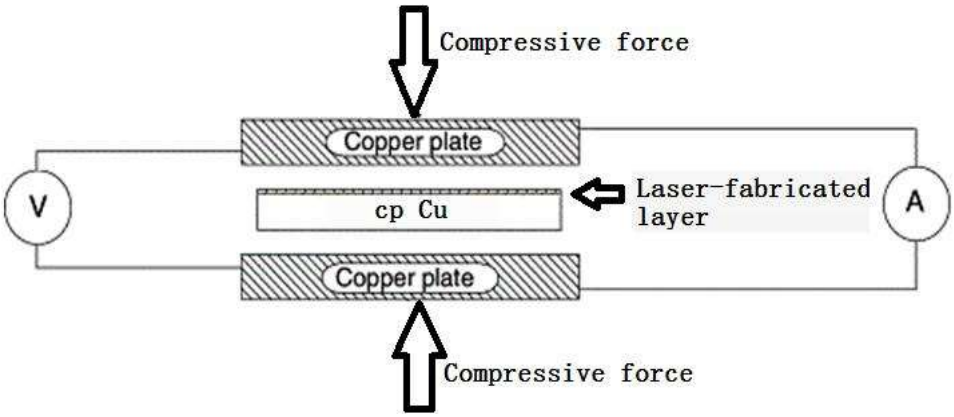

Fig. 1. Schematic of the interfacial contact resistance measurement.

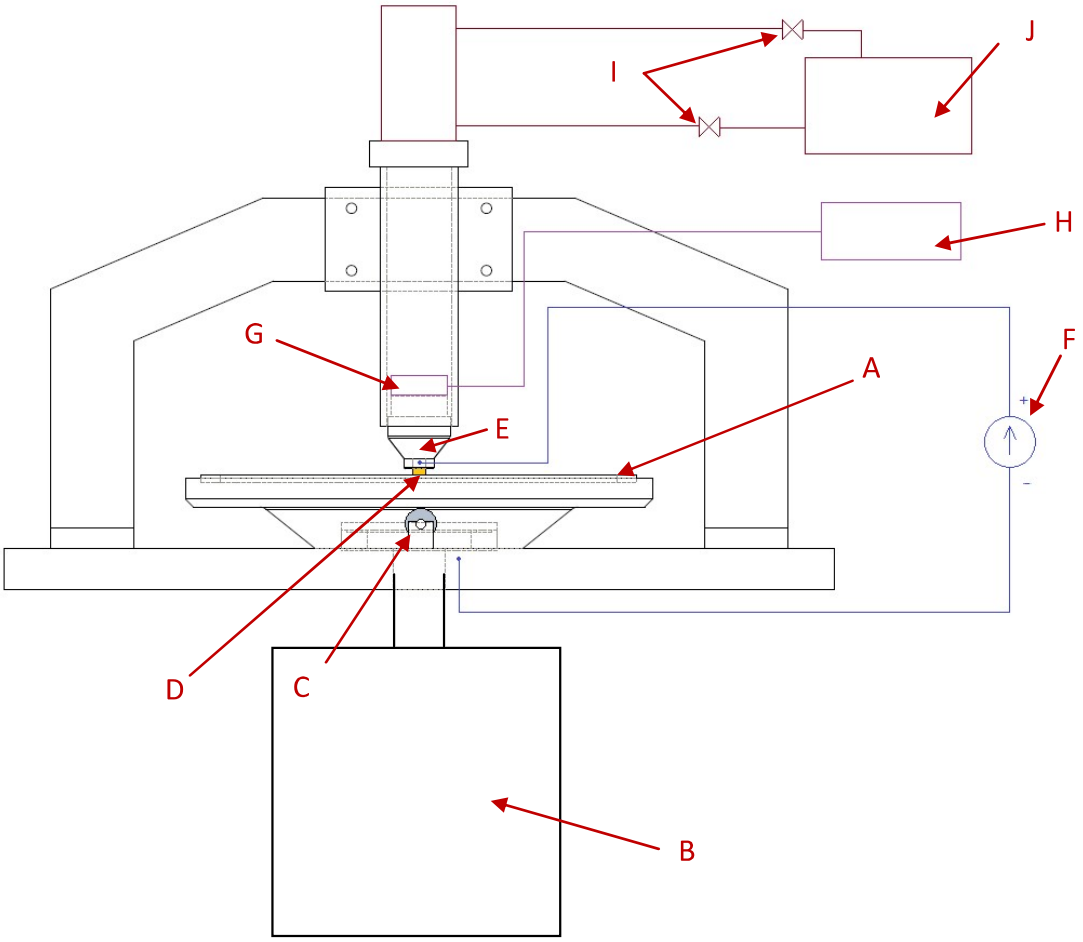

(a)

(b)

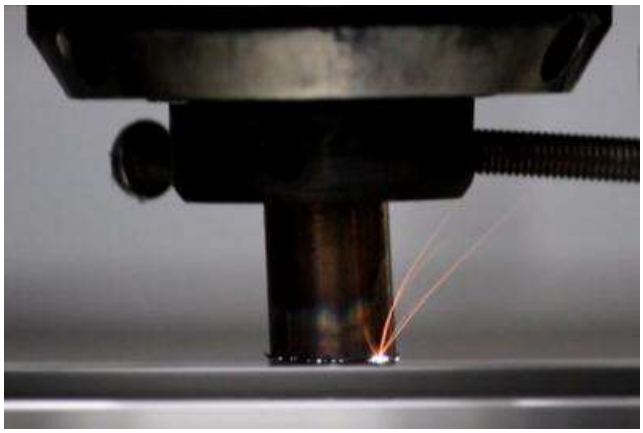

(c)

Fig. 2. (a) Schematic diagram of pin-on-disc tribometer: (A) rotating disc; (B) high-speed motor; (C) bearing support; (D) specimen; (E) specimen holder; (F) power supply; (G) force sensor; (H) manometer; (I) oil control valves; (J) oil pressure pump and tank; (b) overall view of tribometer and (c) electrical sliding wear testing of cp Cu showing arc erosion.

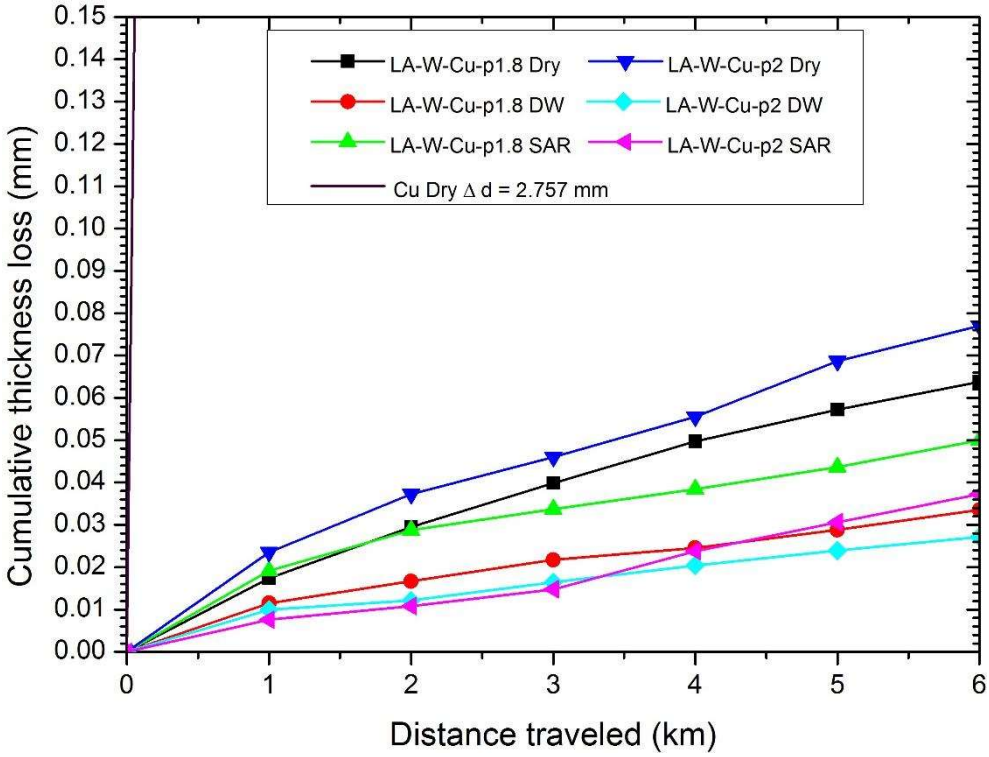
LA-W-Cu-p1.8 Dry
LA-W-Cu-p2 Dry
LA-W-Cu-p1.8 DW
LA-W-Cu-p2 DW
LA-W-Cu-p1.8 SAR
LA-W-Cu-p2 SAR
Cu Dry Δ d = 2.757 mm
Cumulative thickness loss (mm)
Distance traveled (km)
0.00
0.01
0.02
0.03
0.04
0.05
0.06
0.07
0.08
0.09
0.10
0.11
0.12
0.13
0.14
0.15
0
1
2
3
4
5
6

(a)

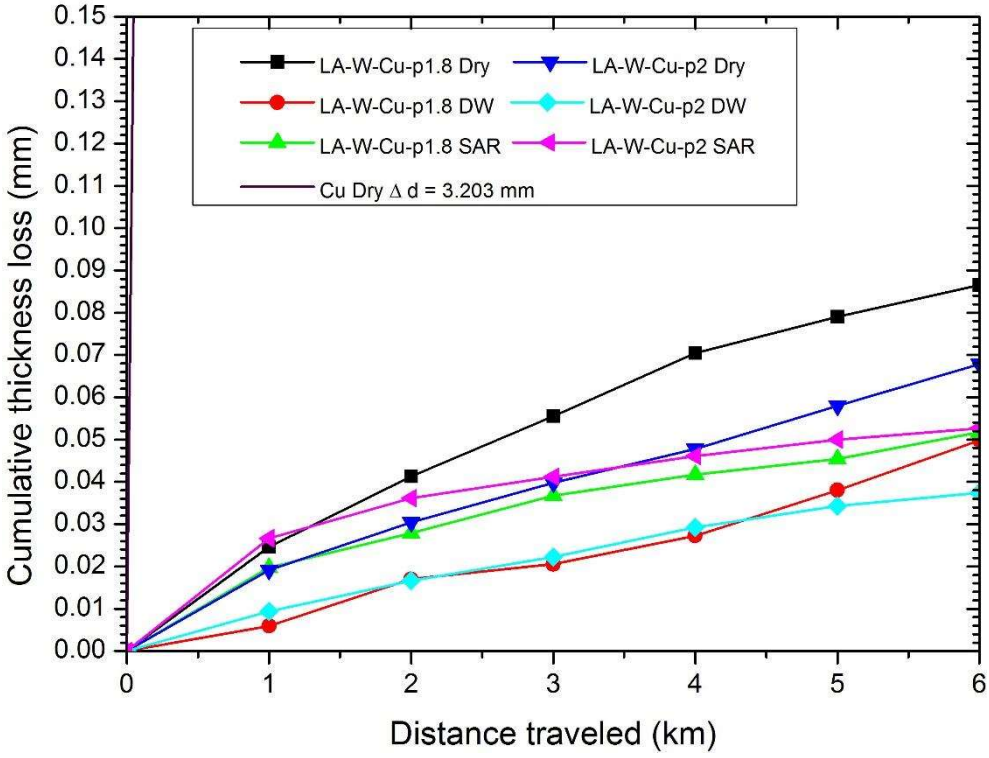
LA-W-Cu-p1.8 Dry
LA-W-Cu-p2 Dry
LA-W-Cu-p1.8 DW
LA-W-Cu-p2 DW
LA-W-Cu-p1.8 SAR
LA-W-Cu-p2 SAR
Cu Dry Δ d = 3.203 mm
Cumulative thickness loss (mm)
Distance traveled (km)
0.00
0.01
0.02
0.03
0.04
0.05
0.06
0.07
0.08
0.09
0.10
0.11
0.12
0.13
0.14
0.15
0
1
2
3
4
5
6

(b)

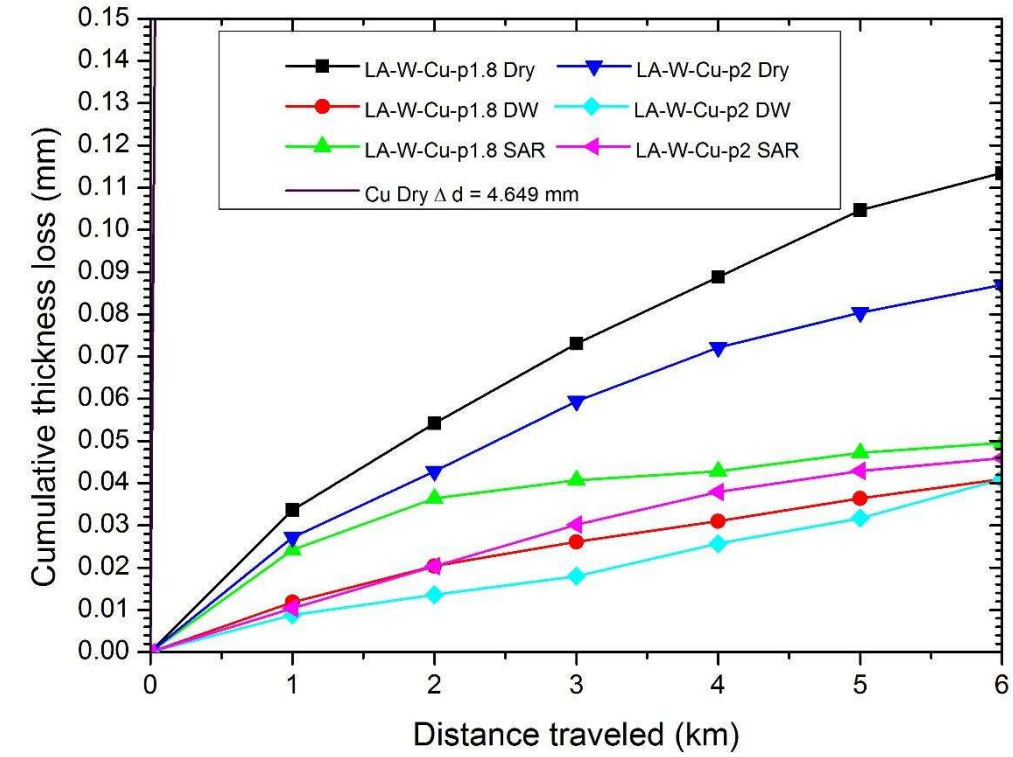

(c)

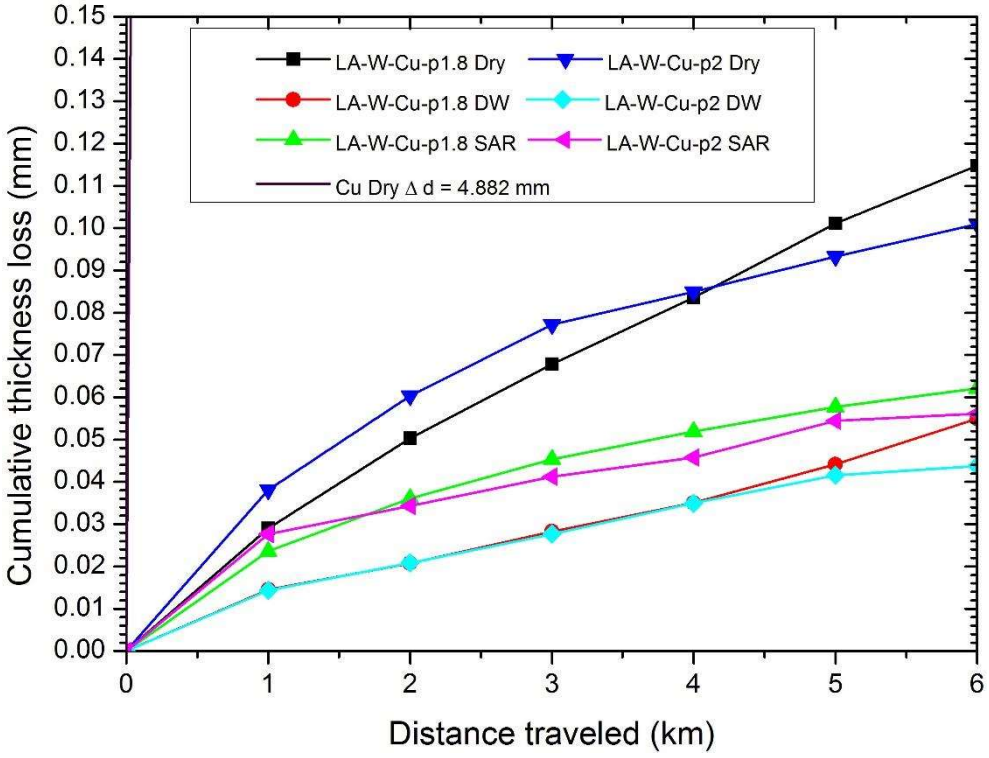

(d)

Fig. 3. Plots of cumulative wear (thickness) loss against distance traveled for laser-fabricated specimens in dry, DW and SAR conditions: (a) 40 km/h, 0 A; (b) 40 km/h, 60 A; (c) 60 km/h, 0 A; and (d) 60 km/h, 60 A.

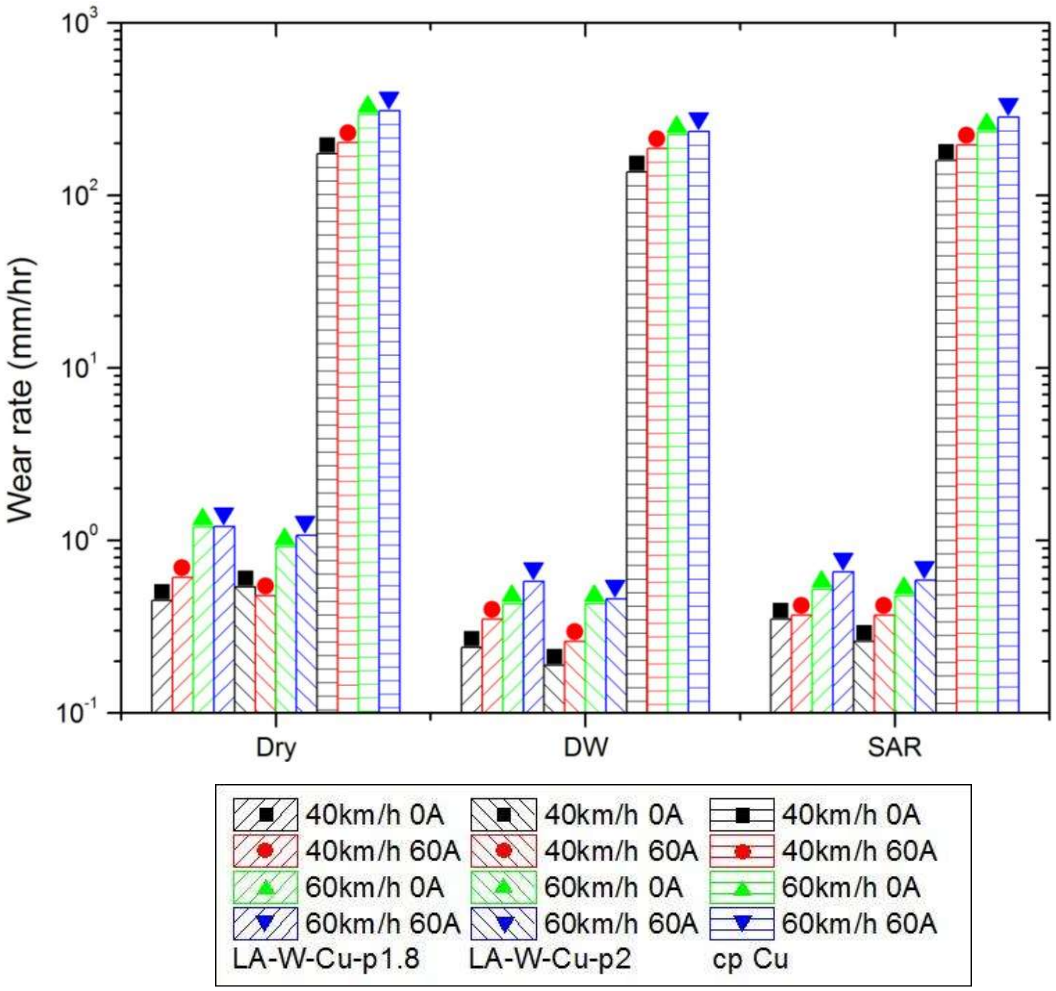

Fig. 4. Electrical wear rates of various laser-fabricated specimens and cp Cu at various test conditions.

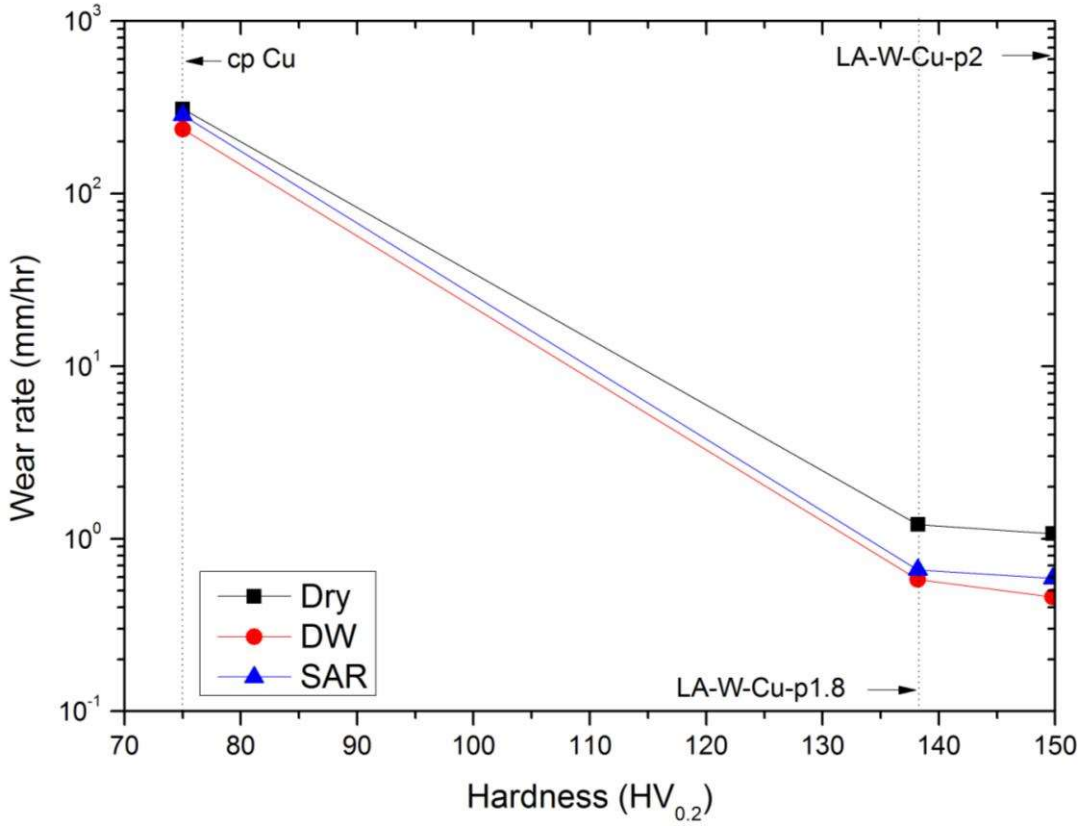

Fig. 5. Plot of wear rate vs hardness for laser-fabricated specimens and cp Cu at 60 km/h and 60 A in dry and wet conditions.

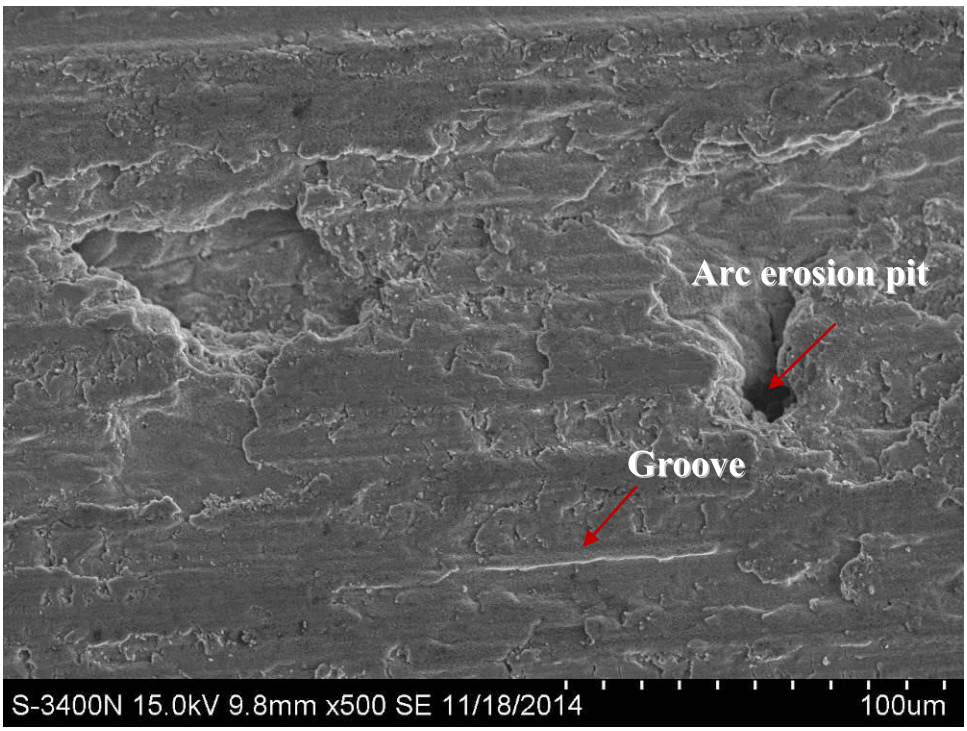
Arc erosion pit
Groove
S-3400N 15.0kV 9.8mm x500 SE 11/18/2014
100um

(a)(i)

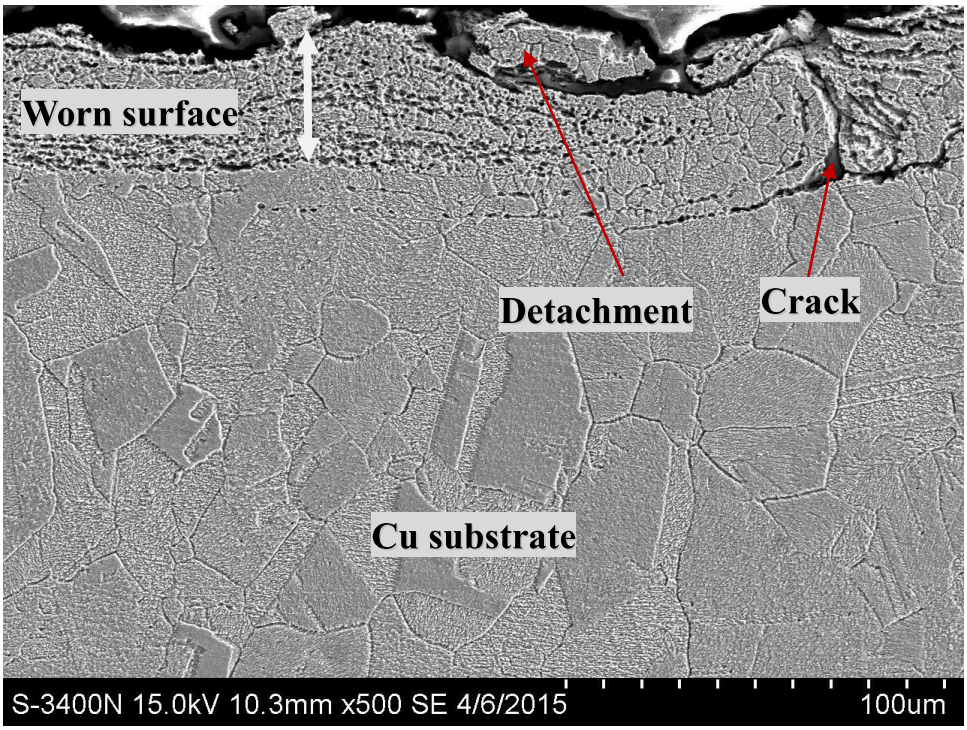
Worn surface
Detachment
Crack
Cu substrate
S-3400N 15.0kV 10.3mm x500 SE 4/6/2015
100um

(a)(ii)

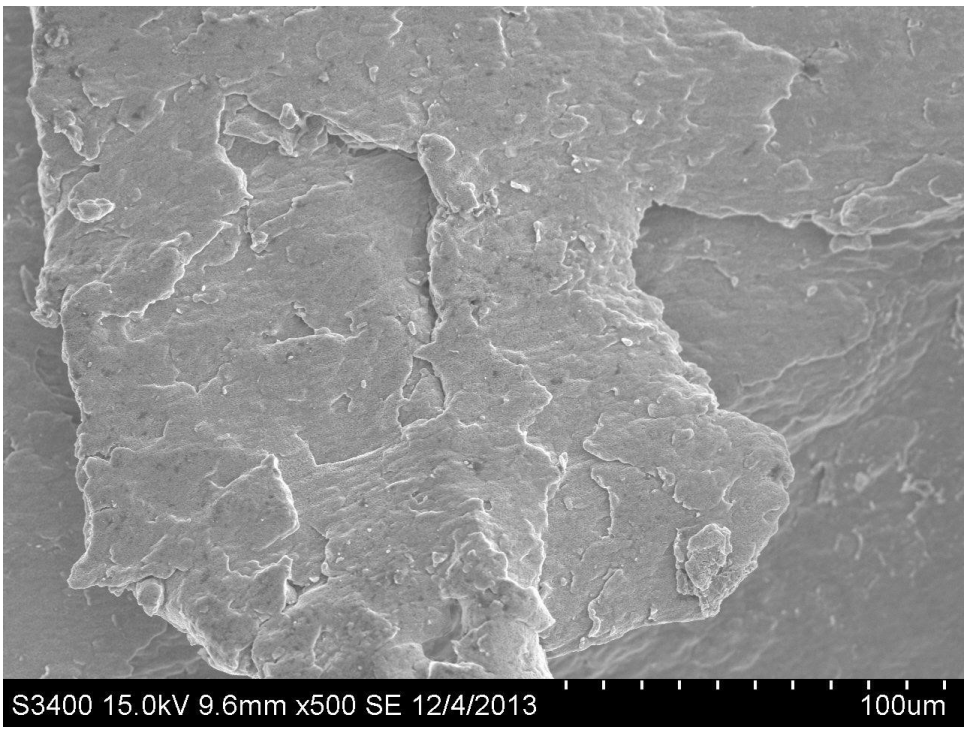

(b) cp Cu, 60 km, 60A, DW

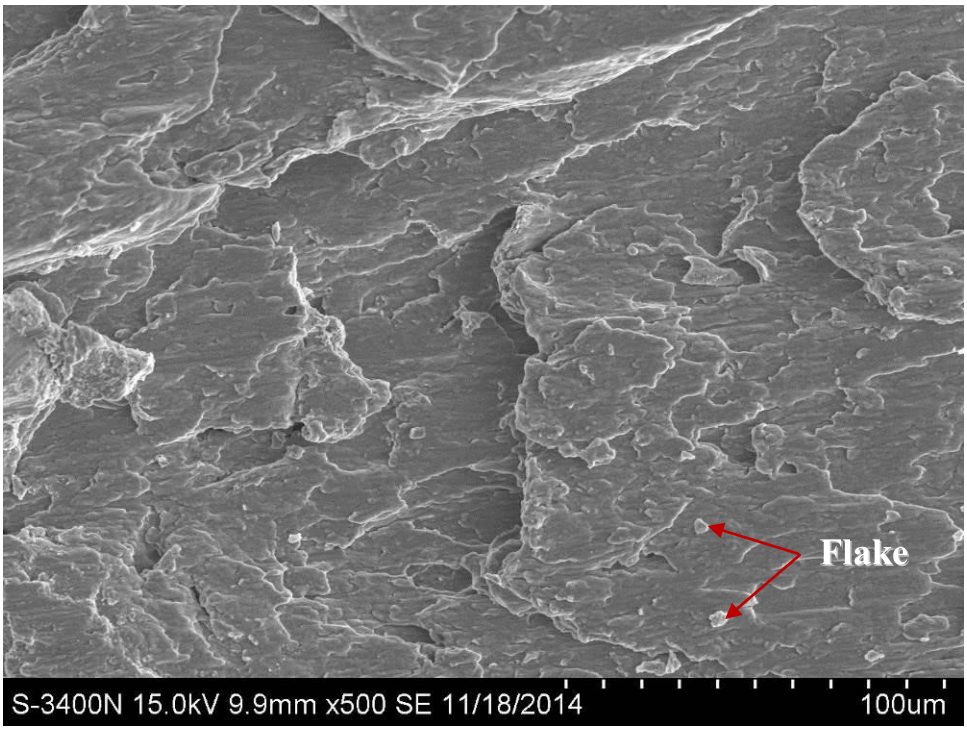

(c) cp Cu, 60 km, 60A, acid rain

Fig. 6. Worn surface and debris of cp Cu at 60 km/h at 60 A in (a) dry condition: (i) surface; (ii) cross-section; (b) DW (surface) and (c) SAR (surface).

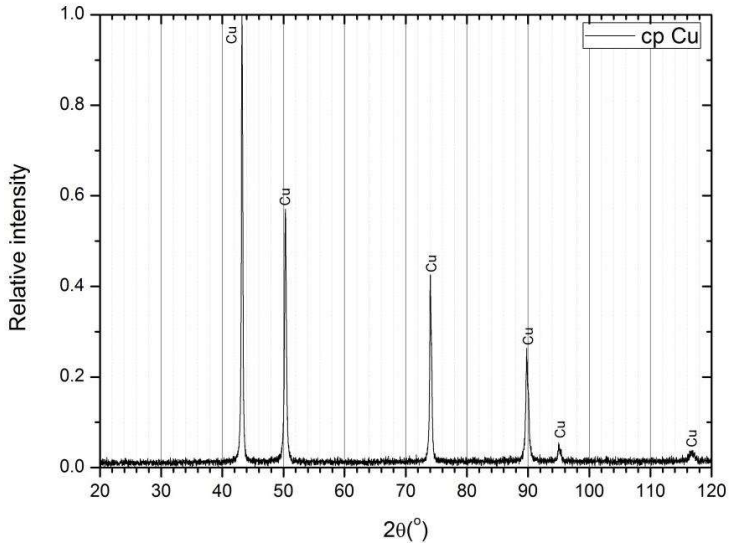

(a)

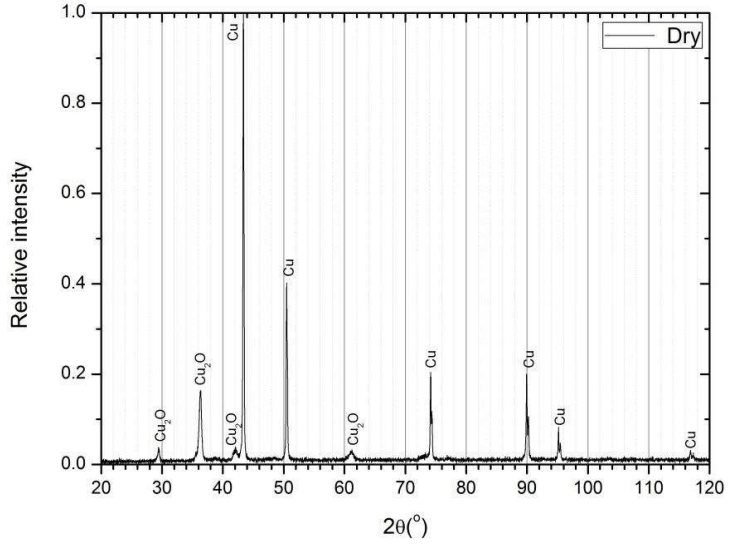

(b)

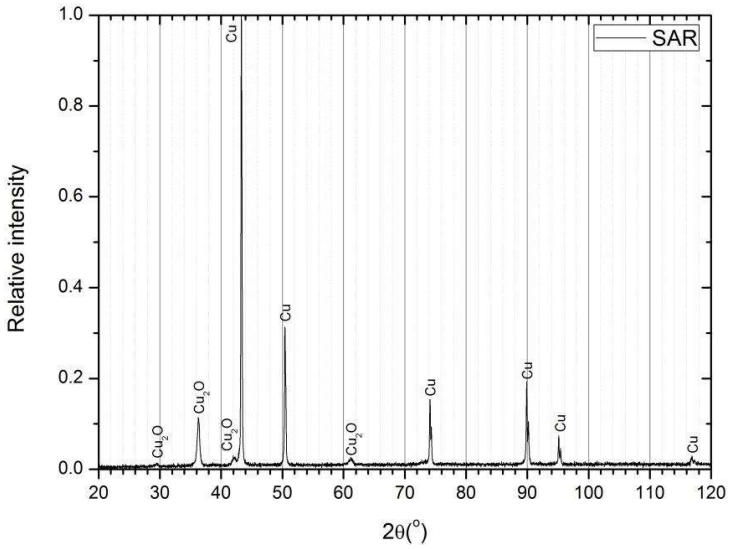

(c)

Fig. 7. XRD patterns of the surface of cp Cu (a) before wear test, (b) after wear test in dry condition at 60

km/h, 60 A and (c) after wear test with SAR at 60 km/h, 60 A.

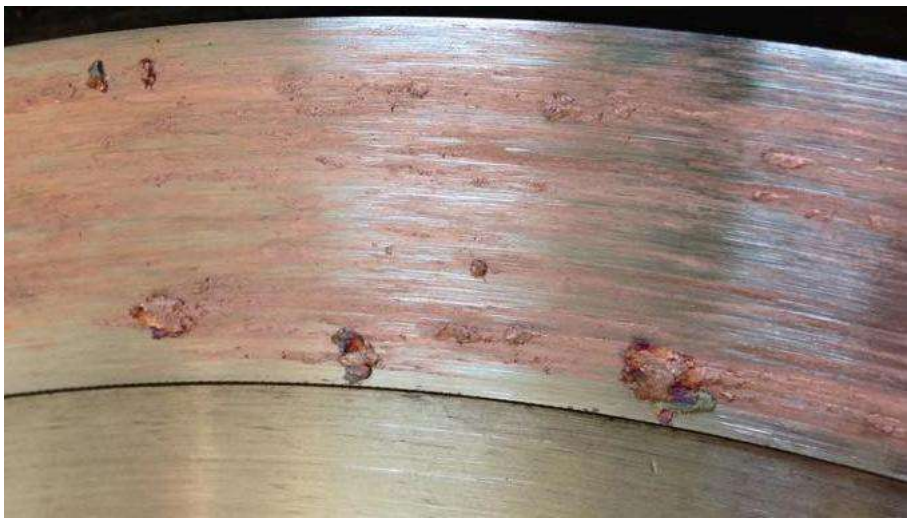

Fig. 8. Worn debris on steel disc after sliding against cp Cu in 60 km/h, 60 A in dry condition.

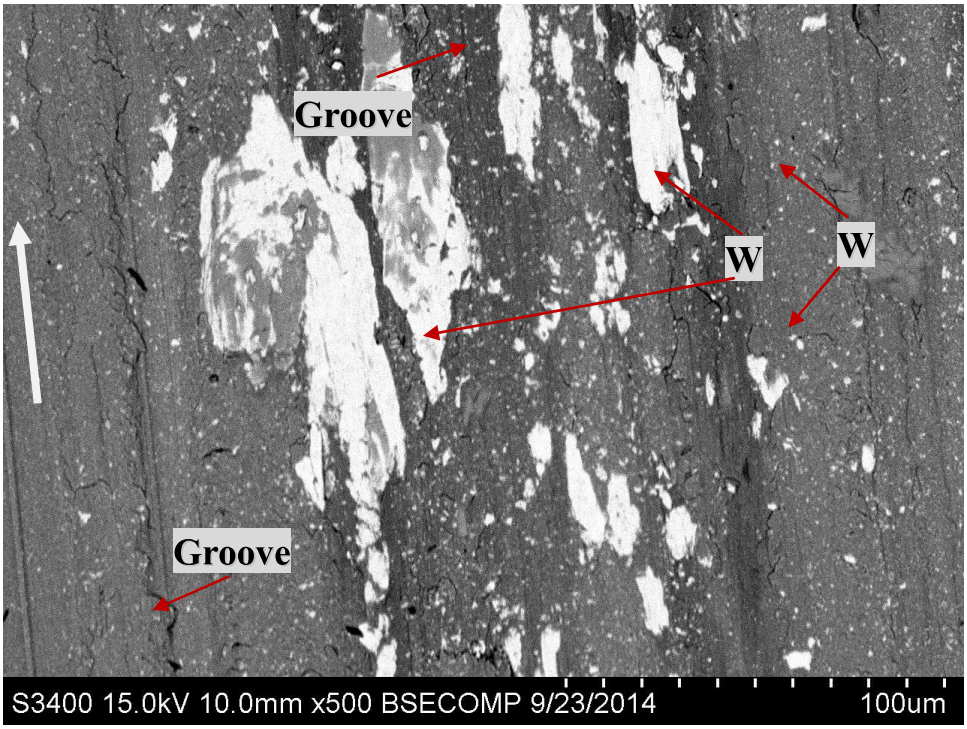
Groove
W
W
Groove
S3400 15.0kV 10.0mm x500 BSECOMP 9/23/2014
100um

(a)

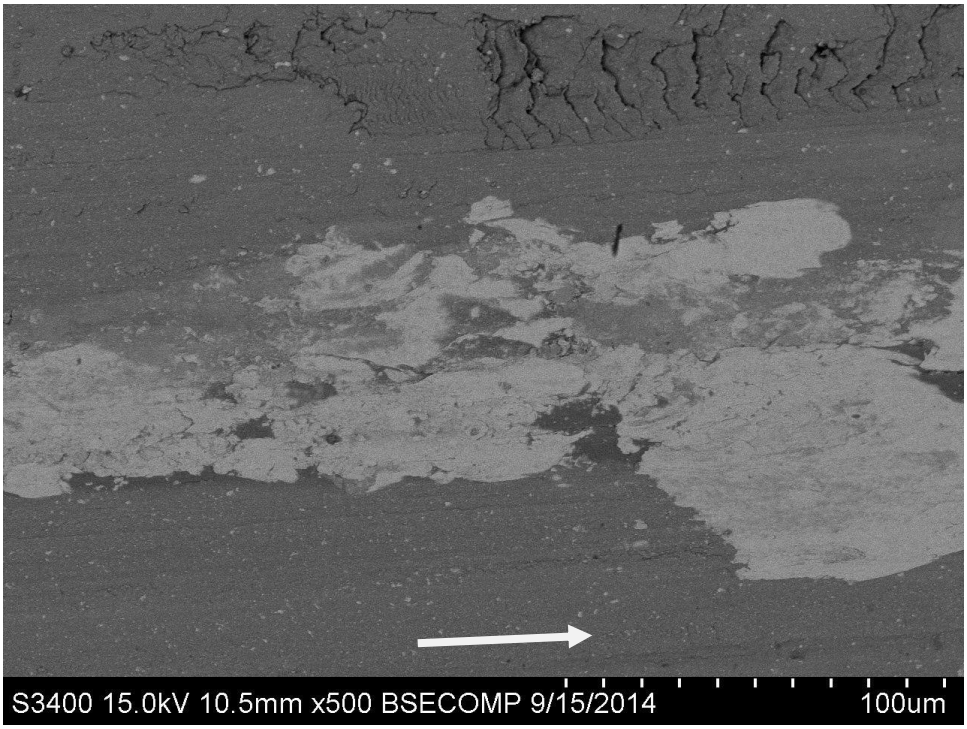
S3400 15.0kV 10.5mm x500 BSECOMP 9/15/2014
100um

(b)(i)

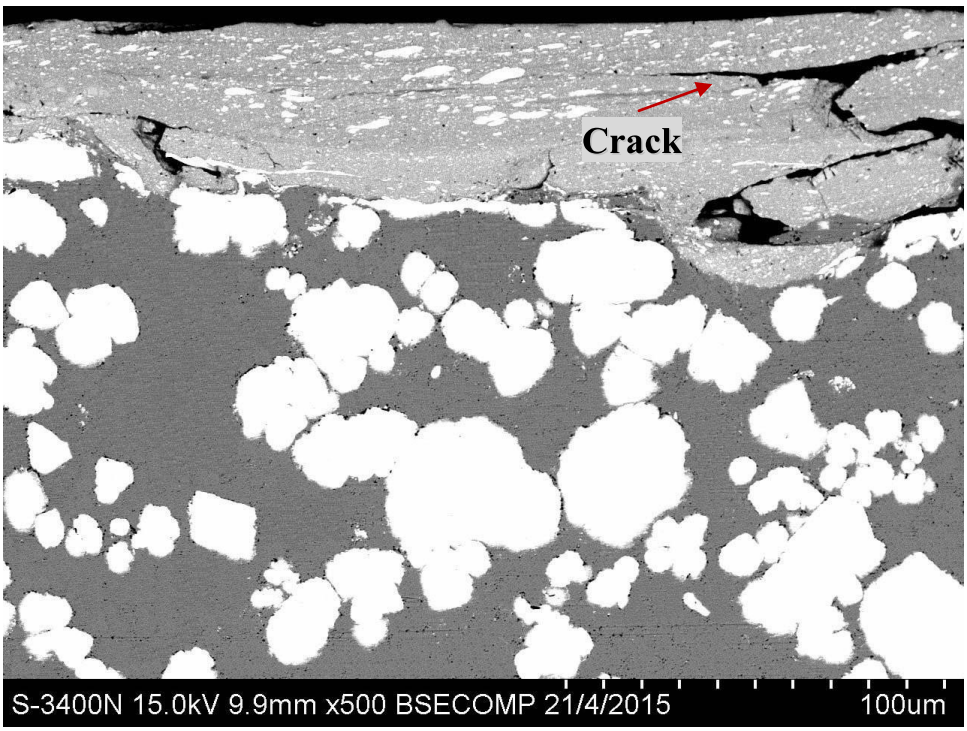

(b)(ii)

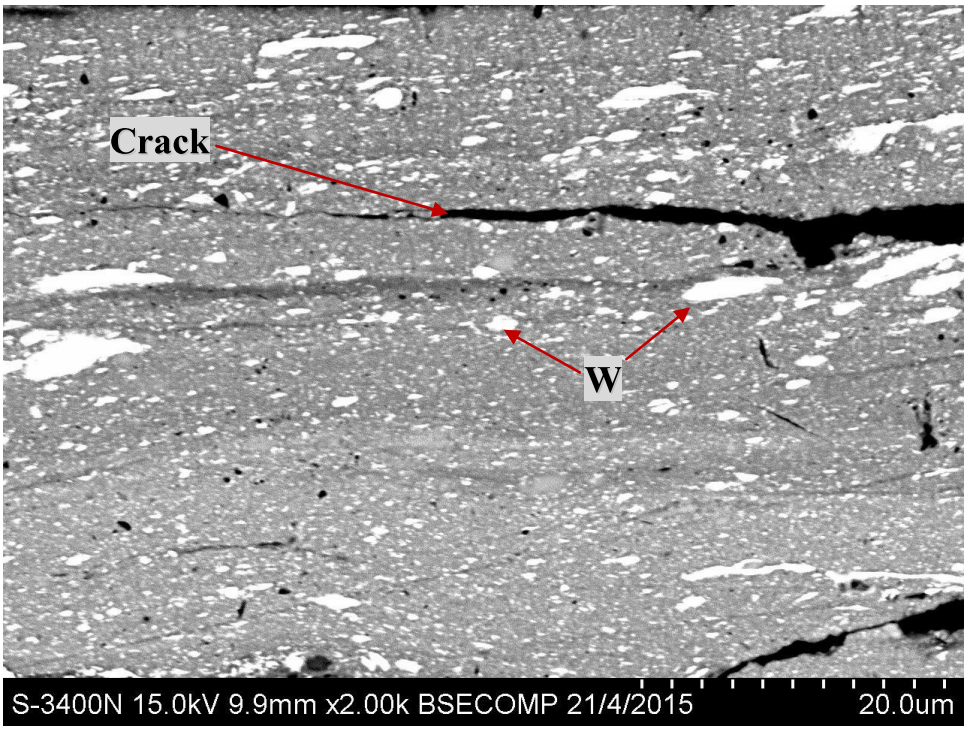

Phase	Cu (wt%)	W (wt%)	Fe (wt%)	O (wt%)
Cu-W-Fe (matrix)	49.3	31.1	10.4	9.2
W (white phase)	0	100	0	0

(b)(iii)

Fig. 9. Worn surface of (a) LA-W-Cu-p1.8 (surface) and (b) LA-W-Cu-p2: (i) surface; (ii) cross-section at low magnification; (iii) cross-section at high magnification at 60 km/h and 60 A in dry condition (white arrow shows the sliding direction).

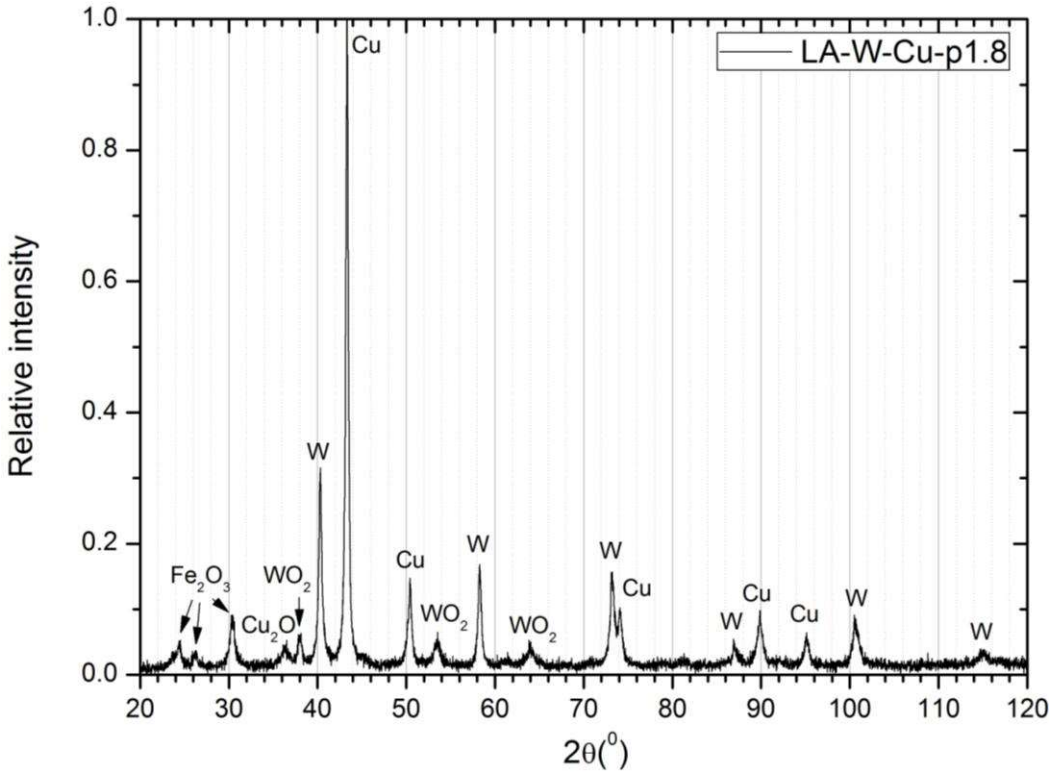

(a)

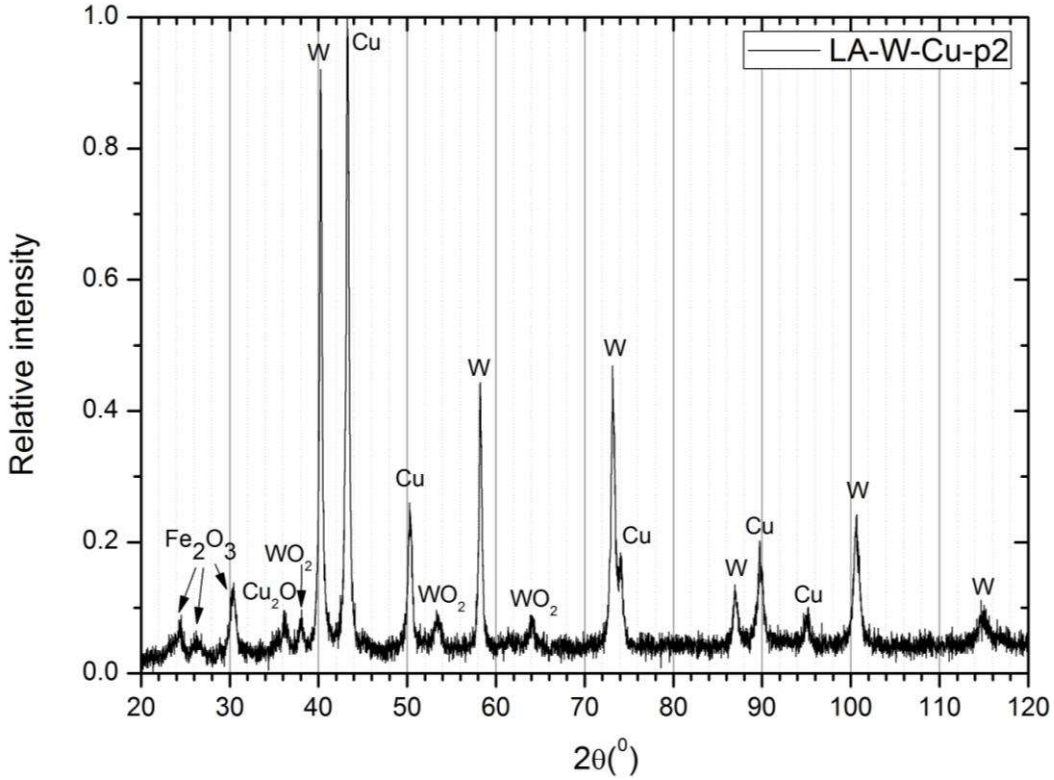

(b)

Fig. 10. XRD patterns of the surface after wear test at 60 km/h and 60 A in dry condition: (a) LA-W-Cu-p1.8 and (a) LA-W-Cu-p2.

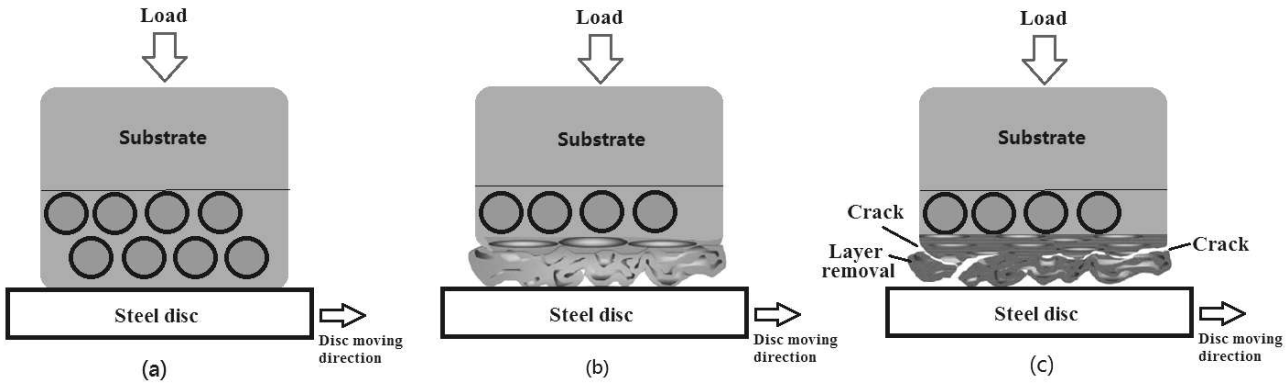

Fig. 11. Schematic representation of the steps of electrical wear mechanism: (a) W-reinforced Cu layer rubbed against the disc (the circles represent the W phases), (b) deformation of surface and formation of severely deformed layer, and (c) initiation and propagation of interface cracks and final delamination.

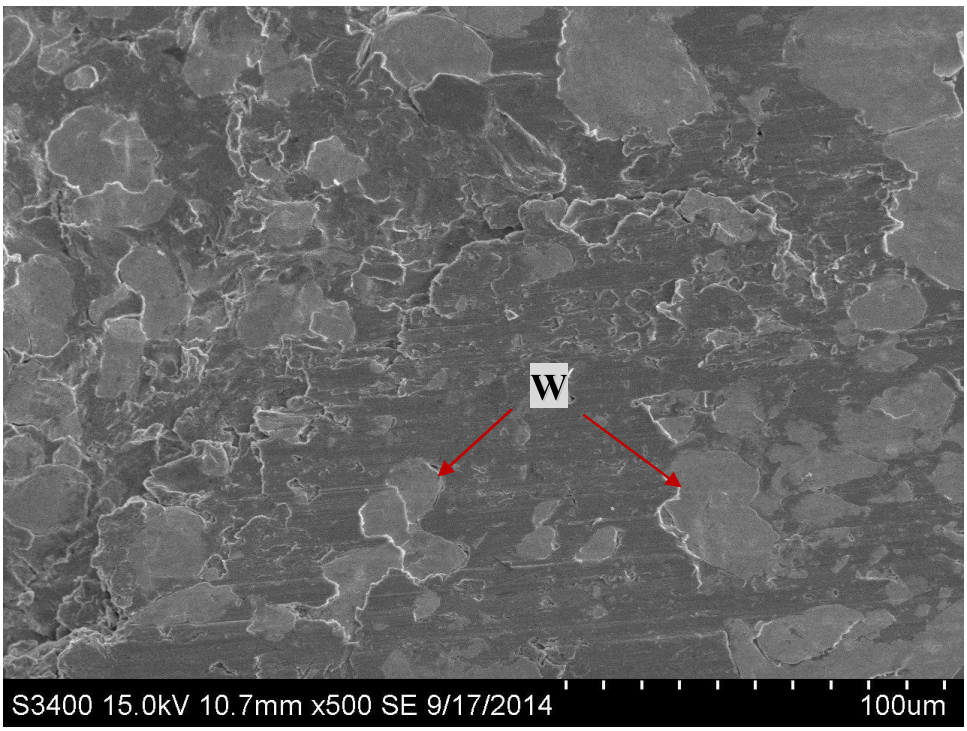

(a)

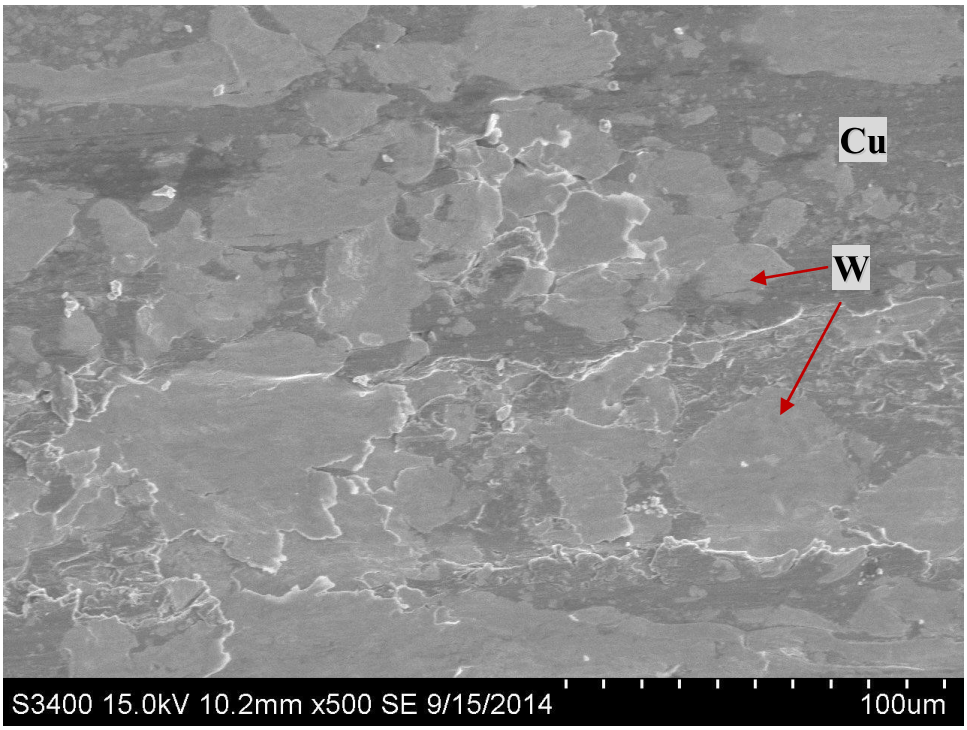

(b)

Fig. 12. Worn surface of (a) LA-W-Cu-p1.8 and (b) LA-W-Cu-p2 at 60 km/h and 60 A in distilled water.

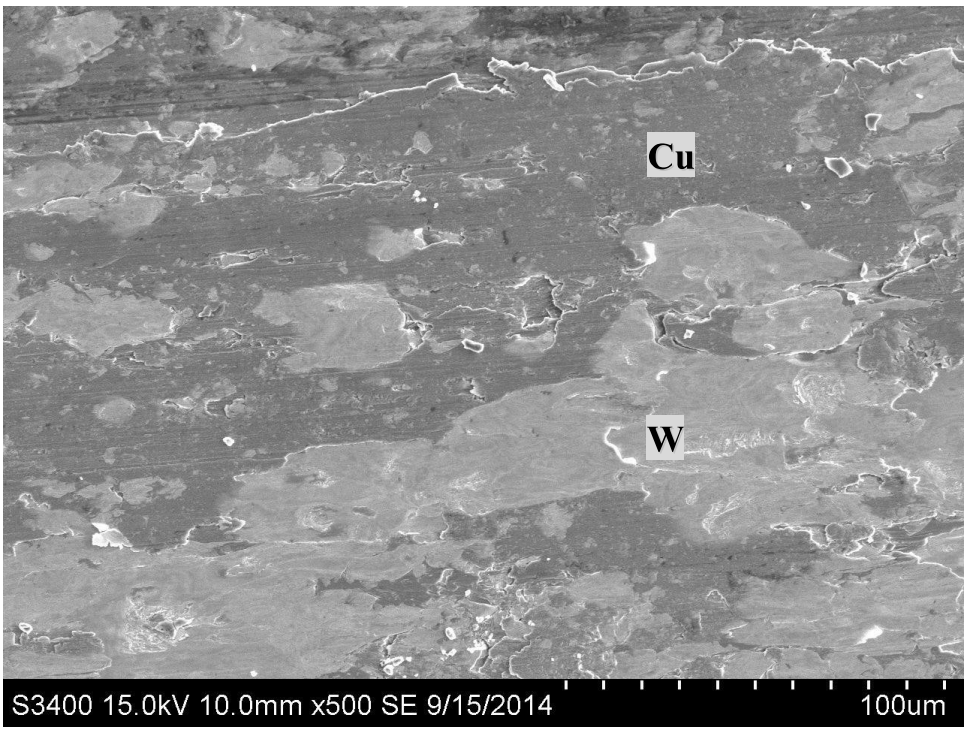
Cu
W
S3400 15.0kV 10.0mm x500 SE 9/15/2014
100um

(a)

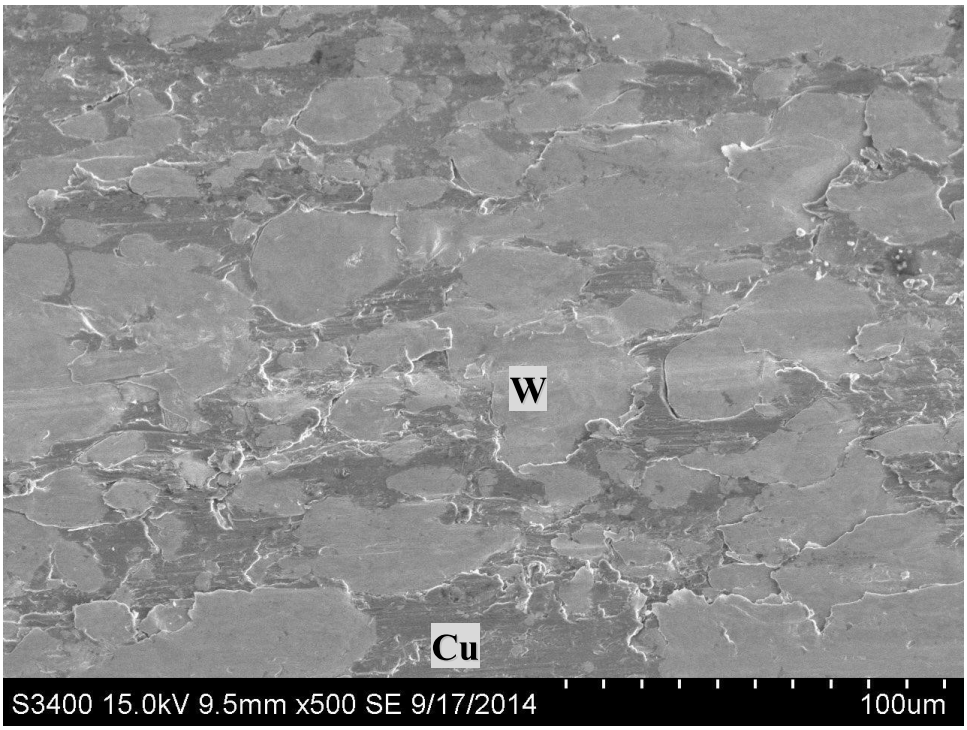
W
Cu
S3400 15.0kV 9.5mm x500 SE 9/17/2014
100um

(b)(i)

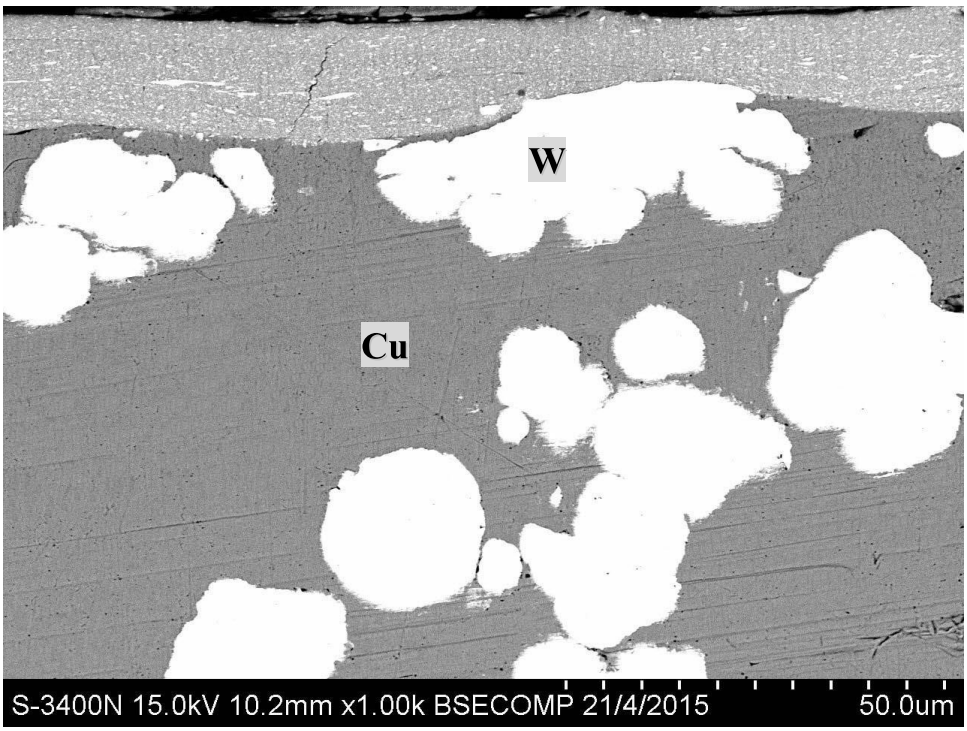

(b)(ii)

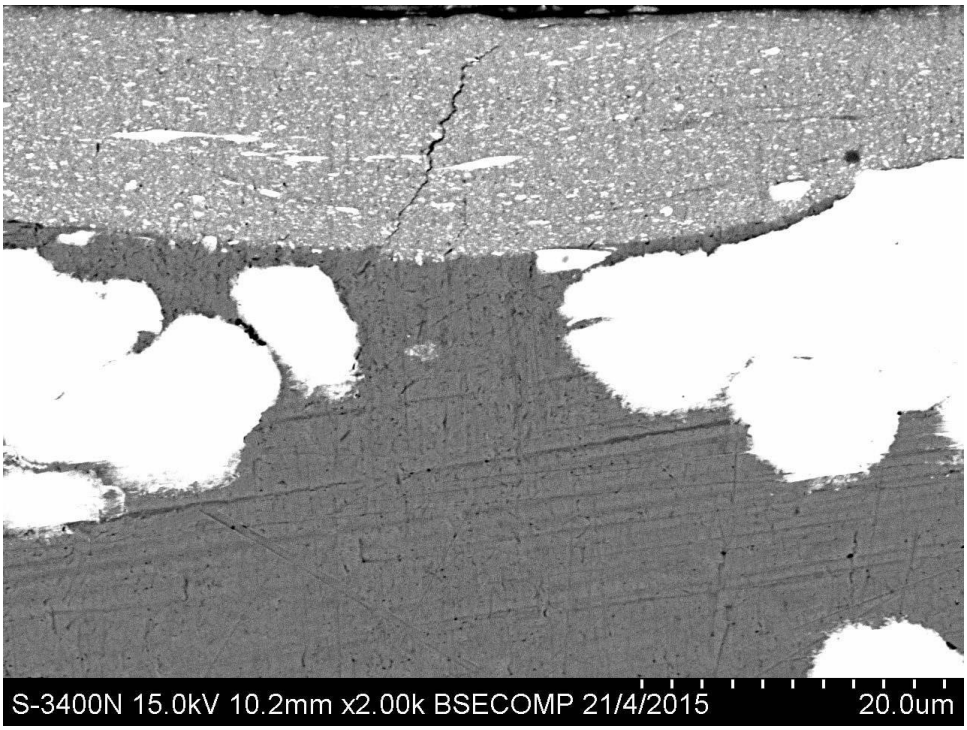

(b)(iii)

Fig. 13. Worn surface of (a) LA-W-Cu-p1.8 and (b) LA-W-Cu-p2 (i) surface; (ii) cross-section at low magnification; (iii) cross-section at high magnification at 60 km/h and 60 A in SAR.

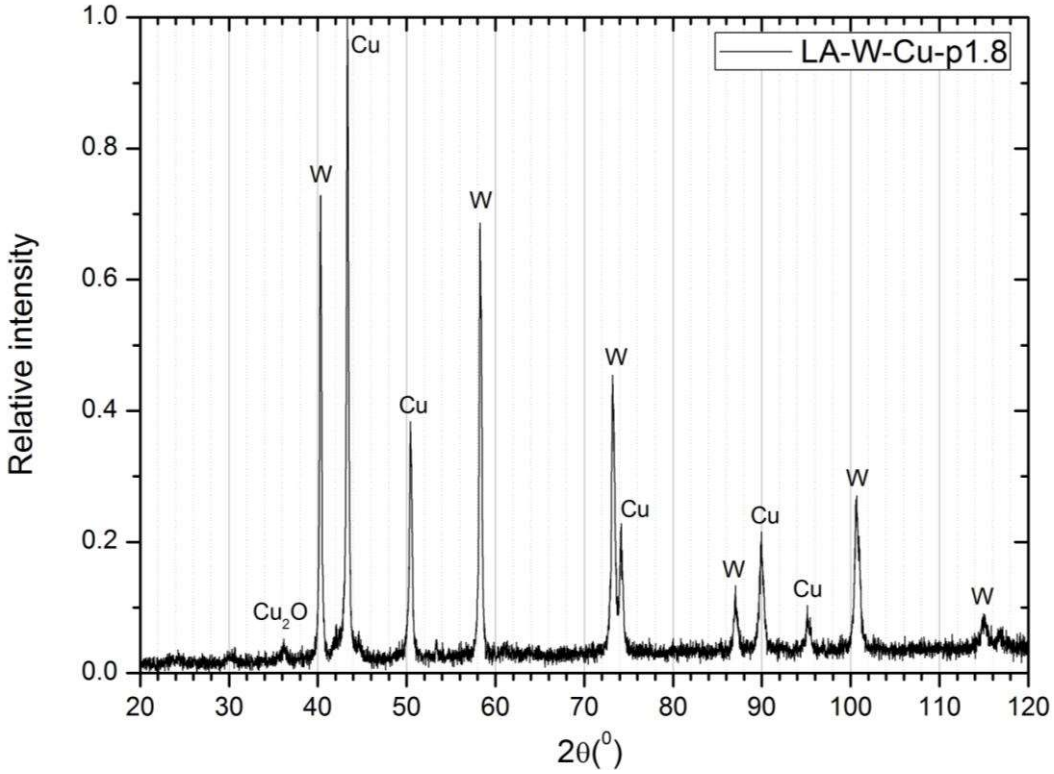
LA-W-Cu-p1.8
Relative intensity
2θ(0)
Cu2O
W
Cu

(a)

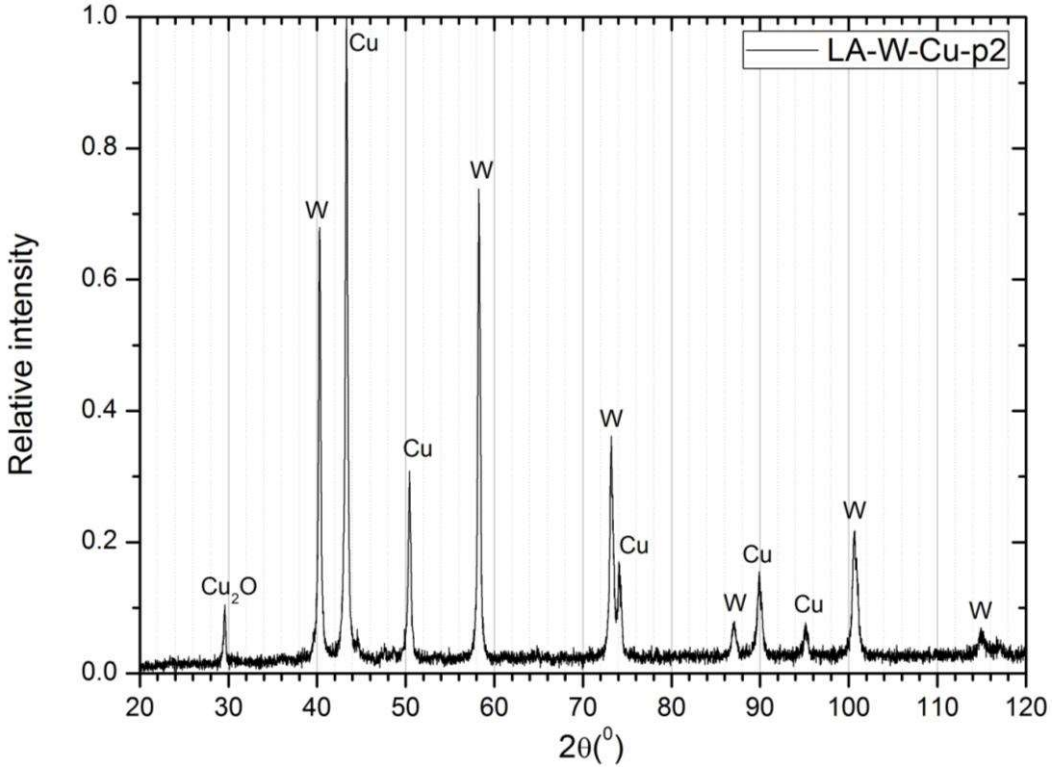
LA-W-Cu-p2
Relative intensity
2θ(0)
Cu2O
W
Cu

(b)

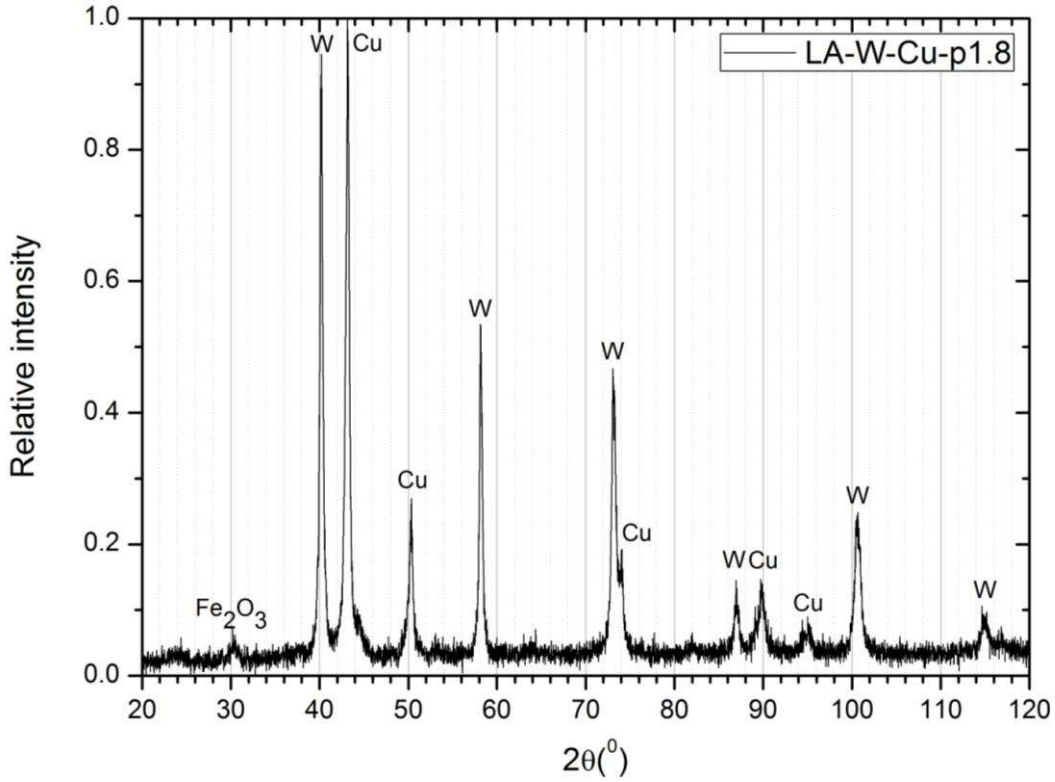

(c)

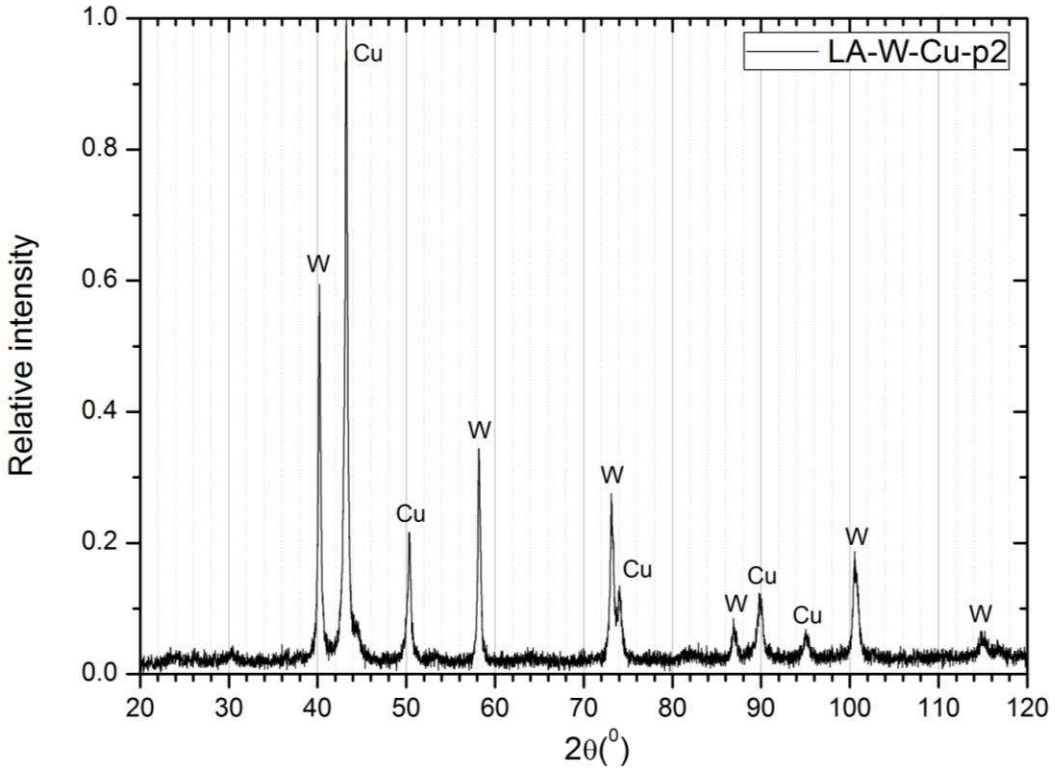

(d)

Fig. 14. XRD patterns of the surface after wear test at 60 km/h and 60 A in wet conditions: (a) LA-W-Cu-p1.8 with DW; (b) LA-W-Cu-p2 with DW; (c) LA-W-Cu-p1.8 with SAR and (d) LA-W-Cu-p2 (SAR).

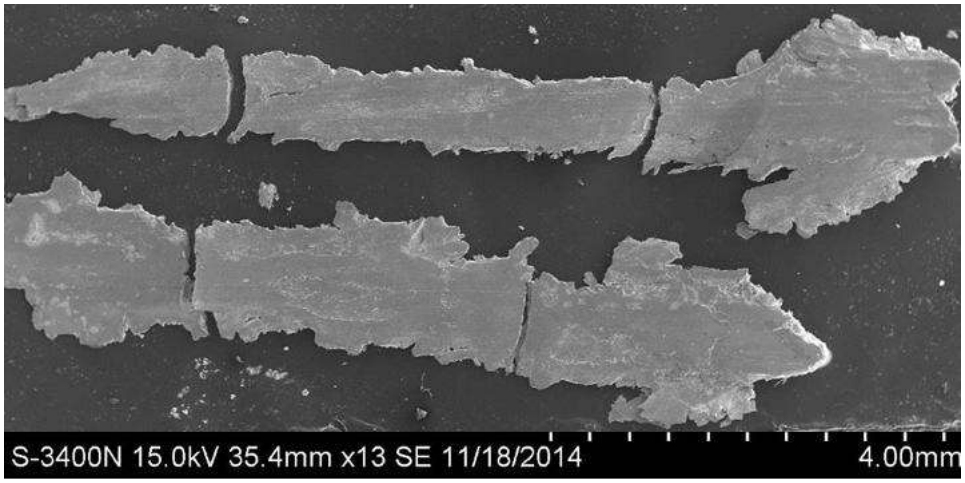
S-3400N 15.0kV 35.4mm x13 SE 11/18/2014
4.00mm

(a)(i)

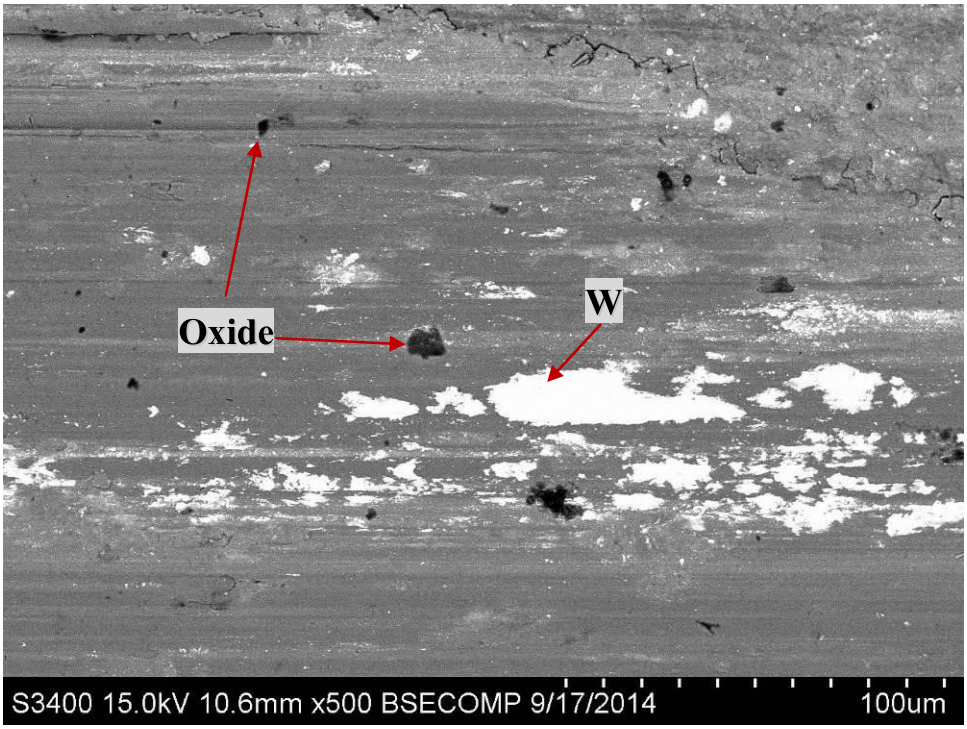
Oxide
W
S3400 15.0kV 10.6mm x500 BSECOMP 9/17/2014
100um

(a)(ii)

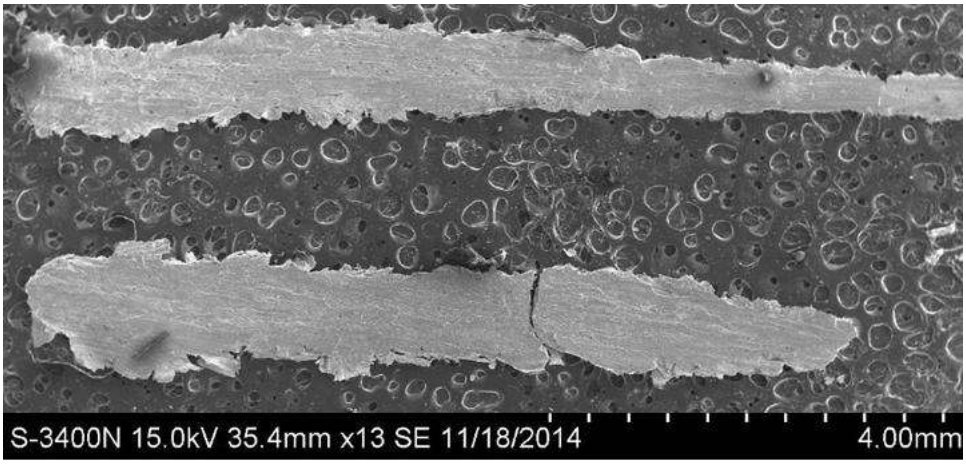
S-3400N 15.0kV 35.4mm x13 SE 11/18/2014
4.00mm

(b)(i)

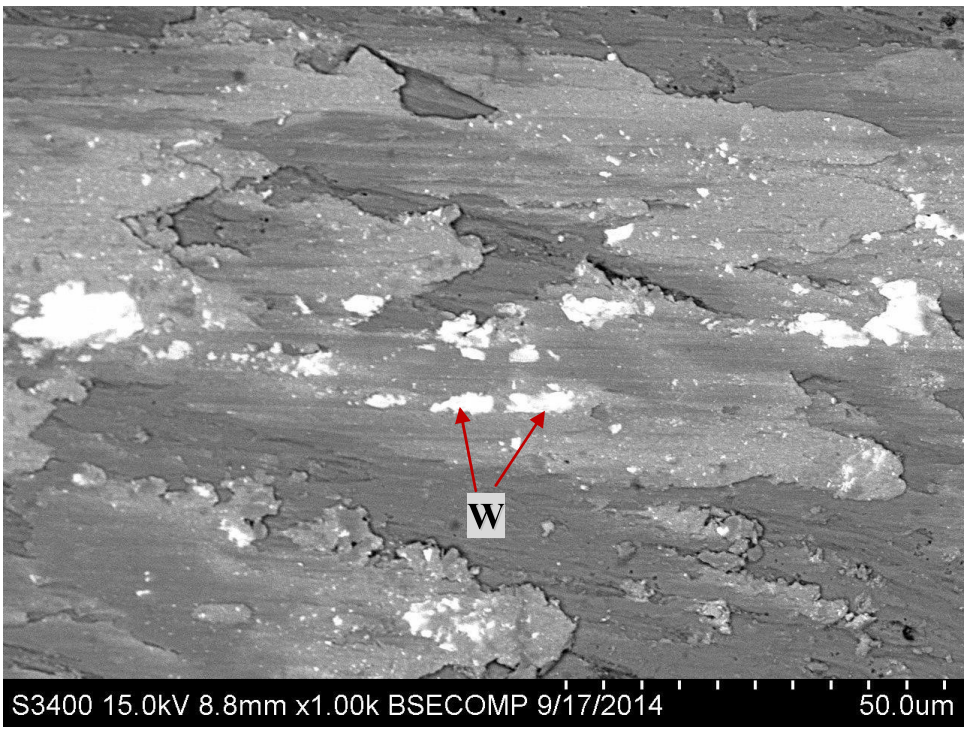

(b)(ii)

Fig. 15. Worn debris of LA-W-Cu-p2 worn at 60 km/h and 60 A (a) in air: (i) overall view; (ii) higher magnification and (b) with SAR: (i) overall view; (ii) higher magnification.

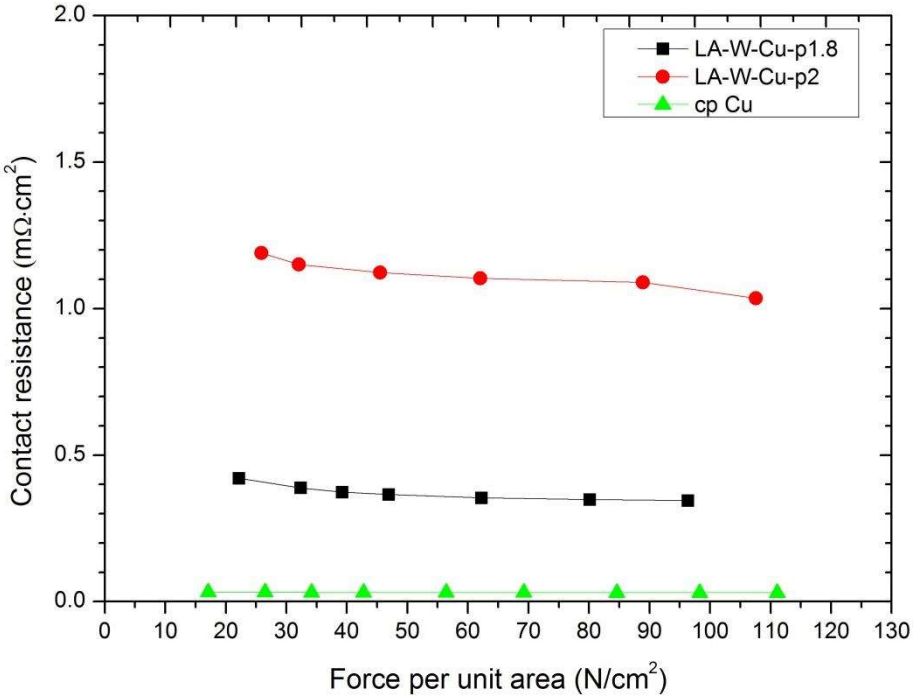

Fig. 16. Plot of interfacial contact resistance versus applied compression force for various specimens.

Figures

Fig. 1. Schematic of the interfacial contact resistance measurement.

Fig. 2. (a) Schematic diagram of pin-on-disc tribometer: (A) rotating disc; (B) high-speed motor; (C) bearing support; (D) specimen; (E) specimen holder; (F) power supply; (G) force sensor; (H) manometer; (I) oil control valves; (J) oil pressure pump and tank; (b) overall view of tribometer and (c) electrical sliding wear testing of cp Cu showing arc erosion.

Fig. 3. Plots of cumulative wear (thickness) loss against distance traveled for laser-fabricated specimens in dry, DW and SAR conditions: (a) 40 km/h, 0 A; (b) 40 km/h, 60 A; (c) 60 km/h, 0 A; and (d) 60 km/h, 60 A.

Fig. 4. Electrical wear rates of various laser-fabricated specimens and cp Cu at various test conditions.

Fig. 5. Plot of wear rate vs hardness for laser-fabricated specimens and cp Cu at 60 km/h and 60 A in dry and wet conditions.

Fig. 6. Worn surface and debris of cp Cu at 60 km/h at 60 A in (a) dry condition: (i) surface; (ii) cross-section; (b) DW (surface) and (c) SAR (surface).

Fig. 7. XRD patterns of the surface of cp Cu (a) before wear test, (b) after wear test in dry condition at 60 km/h, 60 A and (c) after wear test with SAR at 60 km/h, 60 A.

Fig. 8. Worn debris on steel disc after slidng against cp Cu in 60 km/h, 60 A in dry condition.

Fig. 9. Worn surface of (a) LA-W-Cu-p1.8 (surface) and (b) LA-W-Cu-p2: (i) surface; (ii) cross-section at low magnification; (iii) cross-section at high magnification at 60 km/h and 60 A in dry condition (white arrow shows the sliding direction).

Fig. 10. XRD patterns of the surface after wear test at 60 km/h and 60 A in dry condition: (a) LA-W-Cu-p1.8 and (a) LA-W-Cu-p2.

Fig. 11. Schematic representation of the steps of electrical wear mechanism: (a) W-reinforced Cu layer rubbed against the disc (the circles represent the W phases), (b) deformation of surface and formation of severely deformed layer, and (c) initiation and propagation of interface cracks and final delamination.

Fig. 12. Worn surface of (a) LA-W-Cu-p1.8 and (b) LA-W-Cu-p2 at 60 km/h and 60 A in distilled water.

Fig. 13. Worn surface of (a) LA-W-Cu-p1.8 and (b) LA-W-Cu-p2 (i) surface; (ii) cross-section at low

magnification; (iii) cross-section at high magnification at 60 km/h and 60 A in SAR.

Fig. 14. XRD patterns of the surface after wear test at 60 km/h and 60 A in wet conditions: (a) LA-W-Cu-p1.8 with DW; (b) LA-W-Cu-p2 with DW; (c) LA-W-Cu-p1.8 with SAR and (d) LA-W-Cu-p2 (SAR).

Fig. 15. Worn debris of LA-W-Cu-p2 worn at 60 km/h and 60 A (a) in air: (i) overall view; (ii) higher magnification and (b) with SAR: (i) overall view; (ii) higher magnification.

Fig. 16. Plot of interfacial contact resistance versus applied compression force for various specimens.